

A Model for Neutrino Anomalies and IceCube data

Y. H. Ahn

*Department of Physics, Chung-Ang University, Seoul 06974, Korea.**

Sin Kyu Kang

School of Liberal Arts, Seoul Tech, Seoul, 01811 Korea†

Abstract

We interpret the neutrino anomalies in neutrino oscillation experiments and the high energy neutrino events at IceCube in terms of neutrino oscillations in an extension of the standard model where three sterile neutrinos are introduced so as to make two light neutrinos to be Pseudo-Dirac particles and a light neutrino to be a Majorana particle. Our model is different from the so-called $3 + n$ model with n sterile neutrinos suggested to interpret short baseline anomalies in terms of neutrino oscillations. While the Pontecorvo-Maki-Nakagawa-Sakata (PMNS) matrix in $3 + n$ model is simply extended to $n \times n$ unitary matrix, the neutrino mixing matrix in our model is parameterized so as to keep the 3×3 PMNS mixing matrix for three active neutrinos unitary. There are also no flavor changing neutral current interactions leading to the conversion of active neutrinos to sterile ones or vice versa. We derive new forms of neutrino oscillation probabilities containing the new interference between the active and sterile neutrinos which are characterized by additional new parameters Δm^2 and θ . Based on the new formulae derived, we show how the short baseline neutrino anomalies can be explained in terms of oscillations, and study the implication of the high energy neutrino events detected at IceCube on the probe of pseudo-Dirac neutrinos. New phenomenological effects attributed to the existence of the sterile neutrinos are discussed.

PACS numbers:

*Electronic address: axionahn@naver.com

†Electronic address: skkang@seoultech.ac.kr

I. INTRODUCTION

The observation of neutrino oscillations in the atmospheric neutrino¹ Super-Kamiokande [3], the solar neutrino² SNO [5], and the reactor neutrino Daya Bay [6] and RENO [7]³ experiments is one of big discoveries in particle physics since 90's. It implies that neutrinos are massive particles and that the three flavor neutrinos ν_e, ν_μ, ν_τ are mixtures of neutrinos with definite masses ν_i (with $i = 1, 2, \dots$). Although neutrino oscillations among three active neutrino flavors have been confirmed by the analysis based on the experiments mentioned above, there exist several anomalies which are unexpected results coming from short baseline (SBL) experiments such as the reactor antineutrino anomaly [9], the Gallium solar anomaly [10, 11], and the Liquid Scintillator Neutrino Detector (LSND) anomaly [12] (including MiniBooNE anomaly [13]). To resolve those neutrino anomalies in terms of neutrino oscillation, it is required to introduce at least one additional squared-mass difference, Δm_{SBL}^2 , which is much larger than Δm_{Sol}^2 and Δm_{Atm}^2 [9]. This result suggests indication in favor of the possible existence of eV-mass sterile neutrino.

Apart from the anomalous results in accelerator and reactor based neutrino experiments favoring the existence of light sterile neutrino, IceCube experiments [14] announced the observation of very high energy neutrino events. The study for the track-to shower ratio of the subset with energy above 60 TeV coming from IceCube has shown that the events are consistent with the hypothesis that cosmic neutrinos have been seen even though their origin and propagation are still elusive [15]. In order to examine them, we need to discriminate the flavor composition of cosmic neutrinos, which is possible by looking at the topology of the events. But, the current limited statistics does not allow yet to discriminate the initial flavor. It is also widely perceived that the IceCube may serve as astronomical-scale baseline experiment to uncover the oscillation effects due to very tiny mass splitting of the pseudo-Dirac neutrinos. If the oscillation effects induced by pseudo-Dirac neutrinos with very high energy and long trajectory are prominent, then they may affect the observables such as the neutrino flavor composition detected from the ultra-high energy neutrino experiments. Since the current precision on the observation of very high energy neutrino events does not

¹ It has been confirmed by the K2K [1] and MINOS [2] accelerator based experiments.

² It has been confirmed by the reactor neutrino experiment KamLAND [4]

³ See also Double Chooz [8].

exclude such an oscillation effect, it would be meaningful to confront any model for pseudo-Dirac neutrinos realized by introducing sterile neutrinos with the high energy astrophysical neutrino events.

In this work, we construct a model having three sterile neutrinos which make two light neutrinos to be pseudo-Dirac particles and a light neutrino to be Majorana particle. Then, we investigate if the sterile neutrino that makes a light neutrino to be Majorana particle can play a crucial role in resolving the neutrino anomalies from SBL experiments, and study the implication of the very high energy astrophysical neutrino data from IceCube on the probe of the pseudo-Dirac neutrinos. Thus, the goal of this paper is to interpret both SBL neutrino anomalies and astronomical neutrino data observed at IceCube in terms of neutrino oscillations [16–18] in the context of the model we construct.

Our model is different from the so-called $3 + n$ model with n sterile neutrinos suggested to interpret SBL anomalies in terms of neutrino oscillations. While the Pontecorvo-Maki-Nakagawa-Sakata (PMNS) matrix in $3 + n$ model is simply extended to $n \times n$ unitary matrix as in Refs. [19–21], the neutrino mixing matrix in our model is parameterized so as to keep the 3×3 PMNS mixing matrix for three active neutrinos unitary. In this model, there are no flavor changing neutral current interactions leading to the conversion of active neutrinos to sterile ones or vice versa. We will present new forms of neutrino oscillation probabilities modified by introducing new sterile neutrinos. The interference between active flavor and sterile neutrinos due to new additional oscillation parameters Δm^2 and mixing angle θ triggers new oscillation effects which can be responsible for the explanation of SBL neutrino anomalies and very high energy neutrino events at IceCube. Based on the new formulae for neutrino oscillations, we will discuss how SBL neutrino anomalies can be explained or alleviated and consistently accommodate the recent IceCube high energy neutrino events. Constraints on the oscillation parameters coming from solar and atmospheric neutrino data, cosmological observation for the sum of active neutrino masses, effective neutrino mass in β -decay and neutrinoless-double-beta ($0\nu\beta\beta$)-decay experiments will be discussed. Our study based on the terrestrial, atmospheric and solar experiments is similar to that in the so-called $3 + 1$ model in the light that the two very tiny pseudo-Dirac mass splittings are not relevant for those experiments. However, this work includes the study for the implication of IceCube data on the probe of the oscillation effects induced by those two tiny mass splittings while keeping the results for the explanations of SBL neutrino anomalies, atmospheric and solar

neutrino experiments in terms of neutrino oscillations including an eV scale sterile neutrino.

This work is organized as follows. In section II, we discuss our model and study neutrino masses and mixings in the new framework. In section III, we study how the new parameters could be constrained through the cosmological data (the sum of active neutrino masses), and the effective neutrino masses in β -decay and $0\nu\beta\beta$ -decay experiments. In section I,V we develop the new active neutrino oscillation probabilities modified by incorporating new sterile neutrinos. And we study how SBL neutrino anomalies can be explained. In section V, we investigate how new effects due to sterile neutrino in the solar and atmospheric oscillations can be constrained by the SBL $\nu_e(\bar{\nu}_e)$ disappearance and $\nu_\mu(\bar{\nu}_\mu)$ disappearance channels, and examine whether the high energy neutrino events from IceCube data can be interpreted in terms of neutrino oscillation. In section VI we examine astronomical neutrino data observed at IceCube to uncover the oscillation effects of tiny mass splittings. In section VII, we state conclusions by summarizing this work.

II. MASSES AND MIXINGS

Introducing right-handed singlet neutrinos N_R , extra neutrino singlet fermions S , and an $SU(2)_L$ singlet scalar field Ψ . we construct the renormalizable Lagrangian given in the charged lepton basis as [16]

$$-\mathcal{L} = \frac{1}{2}\overline{N_R^c} M_R N_R + \overline{L} \tilde{\Phi} Y_D N_R + \overline{L} \tilde{\Phi} Y_{DS} S + \overline{S^c} \Psi Y_S N_R + \frac{1}{2}\overline{S^c} \mu S + h.c. , \quad (1)$$

where N_R, S are three generations, L stand for $SU(2)_L$ left-handed lepton doublet, $\Phi = (\phi^+, \phi^0)^T$ is the SM Higgs doublet and $\tilde{\Phi} \equiv i\tau_2 \Phi^*$. M_R and μ are Majorana masses for the N_R and S fields, respectively. The above Lagrangian is invariant under $U(1)_{B-L}$ when $\mu, M_R = 0$ by assigning quantum numbers $L : 1, N_R, S : 1, \Psi : -2$, and $\Phi : 0$ under the $U(1)_L$ (or $U(1)_{B-L}$) symmetry. Then, the parameters μ and M_R reflect soft symmetry breaking of $U(1)_L$. Nontrivial vacuum expectation value (VEV) of the scalar field Ψ does not break the electroweak symmetry, but spontaneously breaks the $U(1)_L$ (or $U(1)_{B-L}$) symmetry. Thus the symmetry breaking scale for Ψ can be different from the electroweak scale. Integrating out the heavy Majorana neutrinos in the Lagrangian Eq. (1), we obtain effective Lagrangian

for neutrino sectors given by,

$$\begin{aligned}
-\mathcal{L}_{\text{eff}} = & \overline{\nu}_L \phi^0 Y_{DS} S - \frac{1}{2} \overline{\nu}_L \phi^0 Y_D M_R^{-1} Y_D^T \phi^0 \nu_L^c - \overline{\nu}_L \phi^0 Y_D M_R^{-1} Y_S^T \Psi S \\
& - \frac{1}{2} \overline{S^c} \Psi Y_S M_R^{-1} Y_S^T \Psi S + \frac{1}{2} \overline{S^c} \mu S + \text{h.c.} ,
\end{aligned} \tag{2}$$

where Y_D, Y_S, Y_{DS}, M_R and μ are all 3×3 matrices.

After the scalar fields Φ and Ψ get VEVs and taking S to be right-handed, the Lagrangian for neutrinos in the charged lepton basis reads

$$-\mathcal{L}_\nu = \frac{1}{2} \begin{pmatrix} \overline{\nu}_L^c & \overline{S}_R \end{pmatrix} \mathcal{M}_\nu \begin{pmatrix} \nu_L \\ S_R^c \end{pmatrix} + \frac{g}{\sqrt{2}} W_\mu^- \overline{\ell}_L \gamma^\mu \nu_L + \text{h.c.} + \frac{g}{2 \cos \theta_W} Z_\mu \overline{\nu}_L \gamma^\mu \nu_L , \tag{3}$$

where g is the $SU(2)$ coupling constant, θ_W is the Weinberg angle, $\ell = (e, \mu, \tau)$, $\nu_L = (\nu_e, \nu_\mu, \nu_\tau)$, and $S_R = (S_1, S_2, \dots, S_n)$. The light neutral fermions S_α do not take part in the standard weak interaction and thus are not excluded by LEP results, while the number of active neutrinos coupled with the W^\pm and Z bosons is $N_\nu = 2.984 \pm 0.008$ [22]. After electroweak symmetry breaking, Eq. (3) describes $3 + n$ Majorana neutrinos. In the case of $n = 3$ sterile neutrinos, the 6×6 Majorana neutrino mass matrix is

$$\mathcal{M}_\nu = \begin{pmatrix} M_L & M_D^T \\ M_D & M_S \end{pmatrix} , \tag{4}$$

where the 3×3 mass matrices M_D , M_L , and M_S are those for Dirac masses, left- and right-handed Majorana masses, respectively, given by

$$\begin{aligned}
M_L &= -m_D M_R^{-1} m_D^T, \\
M_D &= m_{DS} - m_D M_R^{-1} m_S^T, \\
M_S &= \mu - m_S M_R^{-1} m_S^T,
\end{aligned} \tag{5}$$

where $m_D = Y_D \langle \phi^0 \rangle$, $m_S = Y_S \langle \Psi \rangle$ and $m_{DS} = Y_{DS} \langle \phi^0 \rangle$. Here we take $M_R \gg m_S \simeq m_D \gg \mu$, and neutrinos become pseudo-Dirac particles when M_D is dominant over M_L and M_S in Eq. (4), which reflects $m_{DS} \gg (m_D m_S)/M_R$. In order to get physical parameters, we perform basis rotations from interaction eigenstates to mass eigenstates [18, 23],

$$\begin{pmatrix} \nu_L \\ S_R^c \end{pmatrix} \rightarrow W_\nu^\dagger \begin{pmatrix} \nu_L \\ S_R^c \end{pmatrix} \equiv \xi_L \tag{6}$$

where ξ_L is the mass eigenstate of neutrino, Here, the 6×6 unitary neutrino transformation matrix W_ν given by,

$$W_\nu = \begin{pmatrix} U_L & 0_3 \\ 0_3 & U_R \end{pmatrix} \begin{pmatrix} V_1 & iV_1 \\ V_2 & -iV_2 \end{pmatrix} V_\nu \quad (7)$$

where

$$V_\nu = \begin{pmatrix} e^{i\phi_1} \cos \theta_1 & 0 & 0 & -e^{i\phi_1} \sin \theta_1 & 0 & 0 \\ 0 & e^{i\phi_2} \cos \theta_2 & 0 & 0 & -e^{i\phi_2} \sin \theta_2 & 0 \\ 0 & 0 & e^{i\phi_3} \cos \theta_3 & 0 & 0 & -e^{i\phi_3} \sin \theta_3 \\ e^{-i\phi_1} \sin \theta_1 & 0 & 0 & e^{-i\phi_1} \cos \theta_1 & 0 & 0 \\ 0 & e^{-i\phi_2} \sin \theta_2 & 0 & 0 & e^{-i\phi_2} \cos \theta_2 & 0 \\ 0 & 0 & e^{-i\phi_3} \sin \theta_3 & 0 & 0 & e^{-i\phi_3} \cos \theta_3 \end{pmatrix}. \quad (8)$$

In the above expression, 0_3 is the 3×3 null matrix, U_R is an unknown 3×3 unitary matrix, $V_1 = \text{diag}(1, 1, 1)/\sqrt{2}$, $V_2 = \text{diag}(e^{i\varphi_1}, e^{i\varphi_2}, e^{i\varphi_3})/\sqrt{2}$ with φ_i being arbitrary phases. The matrices V_1 and V_2 are presonsible for the maximal mixing between active neutrinos and sterile neutrinos. The angle θ_k is introduced thanks to nondegeneracy between M_L and M_S in eq.(4), and thus it is responsible for the deviation of maximal mixing between active neutrino and sterile neutrino, which reflects the breaking of degeneracy of a pair of neutrinos in each generations. It is easily see that maximal mixing between ν_k and S_k^c is recovered in the limit of $\theta_k = 0$. We also note that the 3×3 unitary matrix U_L should be the PMNS neutrino mixing matrix responsible for the mixing among three active neutrinos. Then the neutrino mass matrix \mathcal{M}_ν is diagonalized in the mass eigenstates $(\nu_1, \nu_2, \nu_3, S_1^c, S_2^c, S_3^c)$ basis as

$$W_\nu^T \mathcal{M}_\nu W_\nu = V_\nu^T \begin{pmatrix} \hat{M}_L & \hat{M} \\ \hat{M} & \hat{M}_S \end{pmatrix} V_\nu \equiv \text{diag}(m_{\nu_1}, m_{\nu_2}, m_{\nu_3}, m_{s_1}, m_{s_2}, m_{s_3}). \quad (9)$$

The expression Eq.(9) represents that the Majorana mass matrices M_L and M_S , and Dirac neutrino mass matrix, M_D in Eq.(4) are diagonalized by the mixing matrices U_L and U_R as $\hat{M}_L = U_L^T M_L U_L$, $\hat{M}_S = U_R^T M_S U_R$, and $\hat{M} = U_R^T M_D U_L = \text{diag}(m_1, m_2, m_3)$. To get the real and positive mass squared for the 6 neutrino mass eigenstates, we diagonalize the Hermitian

matrix $\mathcal{M}_\nu \mathcal{M}_\nu^\dagger$ with the help of Eq. (9) as follows,

$$W_\nu^T \mathcal{M}_\nu \mathcal{M}_\nu^\dagger W_\nu^* = V_\nu^T \begin{pmatrix} |\hat{M}|^2 + |\hat{M}||\delta| + \frac{1}{2}(|\hat{M}_L|^2 + |\hat{M}_S|^2) & -\frac{i}{2}(|\hat{M}_L|^2 - |\hat{M}_S|^2) \\ \frac{i}{2}(|\hat{M}_L|^2 - |\hat{M}_S|^2) & |\hat{M}|^2 - |\hat{M}||\delta| + \frac{1}{2}(|\hat{M}_L|^2 + |\hat{M}_S|^2) \end{pmatrix} V_\nu^*, \quad (10)$$

where δ stands for $\delta_k \equiv (\hat{M}_L)_k + (\hat{M}_S^\dagger)_k$ originated from the left- and right-Majorana masses ($k = 1, 2, 3$). From the above equation the mixing parameters θ_k and ϕ_k in Eq. (7) can be obtained

$$\tan 2\theta_k = \frac{|(\hat{M}_L)_k|^2 - |(\hat{M}_S)_k|^2}{2\hat{M}_k|\delta_k|} \quad \text{and} \quad \phi_k = \frac{\pi}{4}. \quad (11)$$

Now, to accommodate both an eV sterile neutrino for a possible solution to the neutrino anomalies [9, 12, 13] and the high energy neutrino events in the IceCube detector [14] to be interpreted as new neutrino oscillations, simultaneously, we assume that $m_{\nu_3} \ll m_{s_3}$ and $m_{\nu_1} \approx m_{s_1}$, $m_{\nu_2} \approx m_{s_2}$,⁴. It is equivalent to take the limit of both $\hat{M}_j \gg |(\hat{M}_L)_j| \gg |(\hat{M}_S)_j|$ (with $j = 1, 2$) and $|(\hat{M}_S)_3| \gg |(\hat{M}_L)_3|$, leading to⁵

$$\delta_{1(2)} \simeq (\hat{M}_L)_{1(2)} \quad \text{and} \quad |\delta_3| \simeq -2m_3 \tan 2\theta_3 \quad (12)$$

which in turn gives $\theta_1 \approx \theta_2 \approx 0$ and $\pi/4 < \theta_3 < \pi/2$. Since the active neutrinos are massive and mixed, the weak eigenstates ν_α (with flavor $\alpha = e, \mu, \tau$) produced in a weak gauge interaction are linear combinations of the mass eigenstates with definite masses. The three neutrino active states emitted by weak interactions are described in terms of the mass eigenstates $\xi_k = (\nu_k \ S_k^c)$ ($k = 1, 2, 3$) as

$$\nu_\alpha = \sum_{k=1}^3 U_{\alpha k} \xi_k \quad (13)$$

⁴ This possibility could theoretically be realized in a non-renormalizable flavor model considering non-Abelian discrete symmetry plus Abelian symmetry, e.g. Refs. [18, 24] where light active neutrino masses are mainly generated by QCD anomalous $U(1)$ symmetry (via Froggatt-Nielson mechanism [25]) while leptonic mixing matrix is produced (through seesaw formula [26]) by non-Abelian discrete symmetry.

⁵ The Dirac masses of first and second generations are much larger than the left(right)-handed Majorana masses of those, while the Dirac mass of third generation is larger than the left(right)-handed Majorana masses of that for $3\pi/8 < \theta_3 < \pi/2$ and smaller for $\pi/4 < \theta_3 \leq 3\pi/8$. For $|(\hat{M}_L)_3| \gg |(\hat{M}_S)_3|$ is not realized due to a requirement $m_{s_3}^2 \gg m_{\nu_3}^2$. See Eq. (18).

with

$$\xi_{k=1,2} = \frac{1}{\sqrt{2}} \begin{pmatrix} 1 & i \end{pmatrix} \begin{pmatrix} \nu_k \\ S_k^c \end{pmatrix} \text{ and } \xi_3 = \frac{1}{\sqrt{2}} \begin{pmatrix} \cos \theta_3 + \sin \theta_3 & \cos \theta_3 - \sin \theta_3 \end{pmatrix} \begin{pmatrix} \nu_3 \\ S_3^c \end{pmatrix}, \quad (14)$$

in which the field redefinitions $\nu_j \rightarrow e^{i\frac{\pi}{4}}\nu_j$, $S_j^c \rightarrow e^{-i\frac{\pi}{4}}S_j^c$ (with $j = 1, 2$) and $\nu_3 \rightarrow e^{i\frac{\pi}{4}}\nu_3$, $S_3^c \rightarrow e^{i\frac{\pi}{4}}S_3^c$ are used. In Eq. (13), U is the 3×3 PMNS mixing matrix U_{PMNS} which is expressed in terms of three mixing angles, $\theta_{12}, \theta_{13}, \theta_{23}$, and three CP -odd phases (one δ_{CP} for the Dirac neutrino and two $\varphi_{1,2}$ for the Majorana neutrino) as [22]

$$U_{\text{PMNS}} = \begin{pmatrix} c_{13}c_{12} & c_{13}s_{12} & s_{13}e^{-i\delta_{CP}} \\ -c_{23}s_{12} - s_{23}c_{12}s_{13}e^{i\delta_{CP}} & c_{23}c_{12} - s_{23}s_{12}s_{13}e^{i\delta_{CP}} & s_{23}c_{13} \\ s_{23}s_{12} - c_{23}c_{12}s_{13}e^{i\delta_{CP}} & -s_{23}c_{12} - c_{23}s_{12}s_{13}e^{i\delta_{CP}} & c_{23}c_{13} \end{pmatrix} P_\nu, \quad (15)$$

where $s_{ij} \equiv \sin \theta_{ij}$, $c_{ij} \equiv \cos \theta_{ij}$ and P_ν is a diagonal phase matrix what is that particles are Majorana ones.

And their mass eigenvalues (real and positive) are given as

$$\begin{aligned} m_{\nu_j}^2 &= m_j^2 + m_j|\delta_j| + \frac{1}{2}(|(\hat{M}_L)_j|^2 + |(\hat{M}_S)_j|^2), \\ m_{\nu_3}^2 &= m_3^2 + \frac{1}{2}(|(\hat{M}_L)_3|^2 + |(\hat{M}_S)_3|^2) + \frac{m_3|\delta_3|}{\cos 2\theta_3}, \\ m_{s_j}^2 &= m_j^2 - m_j|\delta_j| + \frac{1}{2}(|(\hat{M}_L)_j|^2 + |(\hat{M}_S)_j|^2), \\ m_{s_3}^2 &= m_3^2 + \frac{1}{2}(|(\hat{M}_L)_3|^2 + |(\hat{M}_S)_3|^2) - \frac{m_3|\delta_3|}{\cos 2\theta_3}. \end{aligned} \quad (16)$$

The neutrino masses for the first and second generations lift slightly the degeneracy of mass-eigenvalues, and we get almost degenerate pairs of eigenstates with tiny mass differences: the mass-squared differences in each pair $\Delta m_k^2 \equiv m_{\nu_k}^2 - m_{s_k}^2$ (with $k = 1, 2$) are so small that the same mass ordering should apply to both eigenmasses, that is,

$$\Delta m_k^2 = 2m_k|\delta_k| \ll m_{\nu_k}^2 \quad \text{for } k = 1, 2. \quad (17)$$

On the other hand, the mass splitting for third generation is given by

$$\Delta m_3^2 \equiv m_{\nu_3}^2 - m_{s_3}^2 = 2\frac{m_3|\delta_3|}{\cos 2\theta_3}, \quad (18)$$

leading to $-1 < \cos 2\theta_3 < 0$, that is, $\pi/4 < \theta_3 < 3\pi/4$ due to the requirement of $m_{s_3}^2 \gg m_{\nu_3}^2$.

From Eqs. (12) and (18) a possible range of θ_3 can be derived as

$$\frac{\pi}{4} < \theta_3 < \frac{\pi}{2}, \quad (19)$$

in which, especially, for $3\pi/8 < \theta_3 < \pi/2$ the third neutrino pair could be Majorana. As is well-known, because of the observed hierarchy $|\Delta m_{\text{Atm}}^2| = |m_{\nu_3}^2 - (m_{\nu_1}^2 + m_{\nu_2}^2)/2| \gg \Delta m_{\text{Sol}}^2 \equiv m_{\nu_2}^2 - m_{\nu_1}^2 > 0$, and the requirement of a Mikheyev-Smirnov-Wolfenstein (MSW) resonance for solar neutrinos [27], there are two possible neutrino mass spectra: (i) the normal mass ordering (NO) $m_{\nu_1}^2 \approx m_{s_1}^2 < m_{\nu_2}^2 \approx m_{s_2}^2 < m_{\nu_3}^2 \ll m_{s_3}^2$, and (ii) the inverted mass ordering (IO) $m_{\nu_3}^2 < m_{\nu_1}^2 \approx m_{s_1}^2 < m_{\nu_2}^2 \approx m_{s_2}^2 \ll m_{s_3}^2$. We use the following global fit values and 3σ intervals for physics parameters

$$\begin{aligned} \Delta m_{21}^2 &= 7.55_{-0.50}^{+0.59} \times 10^{-5} \text{ eV}^2, & \theta_{12}[^{\circ}] &= 34.5_{-3.0}^{+3.5}, \\ |\Delta m_{31}^2| &= 2.50_{-0.09}^{+0.10} \times 10^{-3} (2.42_{-0.11}^{+0.09} \times 10^{-3}) \text{ eV}^2, & \theta_{23}[^{\circ}] &= 47.7_{-5.9}^{+3.0} (47.9_{-5.6}^{+2.8}), \\ \theta_{13}[^{\circ}] &= 8.45_{-0.45}^{+0.45} (8.53_{-0.43}^{+0.47}), & \delta_{CP}[^{\circ}] &= 238_{-81}^{+111} (281_{-79}^{+68}), \end{aligned} \quad (20)$$

where $\Delta m_{kj}^2 \equiv m_{\nu_k}^2 - m_{\nu_j}^2$, for normal mass ordering (inverted mass ordering) respectively [28]. Using above Eq. (12), we can obtain good approximated forms of $m_{\nu_3}^2$ and $m_{s_3}^2$ in terms of m_3 and θ_3 given as

$$m_{\nu_3}^2 \approx m_3^2 \frac{(1 - \sin 2\theta_3)^2}{\cos^2 2\theta_3}, \quad m_{s_3}^2 \approx m_3^2 \frac{(1 + \sin 2\theta_3)^2}{\cos^2 2\theta_3}. \quad (21)$$

The mass parameter m_3 can be derived from Eqs. (12) and (18) as

$$m_3^2 \simeq \frac{1}{4} \frac{\cos^2 2\theta_3}{\sin 2\theta_3} (\Delta S_{31}^2 - \Delta m_{31}^2), \quad (22)$$

where $\Delta S_{kj}^2 \equiv m_{s_k}^2 - m_{s_j}^2$. Clearly, within the range Eq. (19) a value of θ_3 going around $\pi/4$ can realize the inverted mass hierarchy (IH), $m_{\nu_2} > m_{\nu_1} \gg m_{\nu_3}$, while a value around $\pi/2$ favors the degenerate normal mass ordering (DNO), $m_{\nu_3} \gtrsim m_{\nu_2} \gtrsim m_{\nu_1}$, and degenerate inverted mass ordering (DIO), $m_{\nu_2} \gtrsim m_{\nu_1} \gtrsim m_{\nu_3}$. Hence, in this picture, neutrino oscillations can be described by ten parameters: six (two independent Δm_{Atm}^2 , Δm_{Sol}^2 , three mixing angles $\theta_{12}, \theta_{13}, \theta_{23}$, and a Dirac CP phase δ_{CP}) associated with the standard three-active neutrino oscillations [22] and four ($\Delta m_{1,2}^2$, $\Delta S_{31}^2, \theta_3$) responsible for the new oscillations involving sterile neutrino ⁶.

Assuming $\Delta m_{1(2)}^2 \ll \Delta m_{\text{Sol}}^2 \ll |\Delta m_{\text{Atm}}^2| \ll |\Delta m_3^2|$, we expect that the effects of the pseudo-Dirac neutrinos for the first and second generations can be detected through ABL oscillation experiments [16, 18], whereas that for the third generation can be measured through

⁶ Δm_3^2 is determined via $\Delta m_3^2 = \Delta m_{3i}^2 - \Delta S_{3i}^2 \approx -\Delta S_{3i}^2$ for $\Delta S_{3i}^2 \gg |\Delta m_{3i}^2|$ in the limit $\Delta m_i^2 \rightarrow 0$ with $i = 1, 2$.

SBL oscillation experiments (or possibly long baseline oscillation experiments). The mass splittings will manifest themselves through very long wavelength oscillations characterized by the $\Delta m_{1(2)}^2$ as well as very short wavelength oscillations characterized by the Δm_3^2 . The mass splitting Δm_3^2 could be limited by the active neutrino mass orderings with a requirement of $|\Delta m_3^2| \gg \Delta m_{\text{Atm}}^2$:

$$|\Delta m_3^2| \gg 2.6 \times 10^{-3} \text{ eV}^2, \quad (23)$$

where the hierarchical mass orderings ($m_{\nu_2} > m_{\nu_1} \gg m_{\nu_3}$ and $m_{\nu_3} \gg m_{\nu_2} > m_{\nu_1}$) are used. And since the mass splittings $\Delta m_{1(2)}^2$ can modify the large mixing angle solution of the solar neutrino oscillations, they should be limited and detailed fits imply a bound [29]

$$\Delta m_{1(2)}^2 < 1.8 \times 10^{-12} \text{ eV}^2 \text{ at } 3\sigma. \quad (24)$$

Thus, we simply ignore $\Delta m_{1(2)}^2$ in the study of short baseline neutrino oscillations.

III. CONSTRAINTS ON THE NEW OSCILLATION PARAMETERS

In this section, we present how the mixing parameters θ_3 and ΔS_{31}^2 (or Δm_3^2 , actually, the mass scale of the third generation of sterile neutrino) could be constrained through the sum of three active neutrinos $\sum m_\nu$ [30–32], and the effective neutrino masses in β -decay [33] as well as $0\nu\beta\beta$ -decay [34] experiments.

Oscillation experiments are unfortunately insensitive to the absolute scale of neutrino masses. Whereas cosmology is mostly sensitive to the total energy density in neutrinos, directly proportional to the sum of the active neutrino masses $\sum m_\nu = m_{\nu_1} + m_{\nu_2} + m_{\nu_3}$. We will mainly focus on cosmological observations as a probe of the absolute neutrino mass scale. Using Eq. (22), the active neutrino masses in Eq. (16) can be expressed in terms of the new parameters ($\Delta S_{31}^2, \theta_3$) and the two known mass squared differences of oscillation experiments ($\Delta m_{\text{Atm}}^2, \Delta m_{\text{Sol}}^2$) as

$$\begin{aligned} m_{\nu_1}^2 &= (\Delta S_{31}^2 - \Delta m_{\text{Atm}}^2 - \frac{1}{2}\Delta m_{\text{Sol}}^2) \frac{(1 - \sin 2\theta_3)^2}{4 \sin 2\theta_3} - \Delta m_{\text{Atm}}^2 - \frac{1}{2}\Delta m_{\text{Sol}}^2, \\ m_{\nu_2}^2 &= (\Delta S_{31}^2 - \Delta m_{\text{Atm}}^2 - \frac{1}{2}\Delta m_{\text{Sol}}^2) \frac{(1 - \sin 2\theta_3)^2}{4 \sin 2\theta_3} - \Delta m_{\text{Atm}}^2 + \frac{1}{2}\Delta m_{\text{Sol}}^2, \\ m_{\nu_3}^2 &= (\Delta S_{31}^2 - \Delta m_{\text{Atm}}^2 - \frac{1}{2}\Delta m_{\text{Sol}}^2) \frac{(1 + \sin 2\theta_3)^2}{4 \sin 2\theta_3}. \end{aligned} \quad (25)$$

Cosmological and astrophysical measurements provide powerful constraints on the sum of neutrino masses complementary to those from accelerators and reactors. There are several upper limits on the sum of active neutrino masses coming from the CMB data and weak lensing data:

$$0.06 \text{ [eV]} \lesssim \sum_i m_{\nu_i} < \begin{cases} 0.340 \sim 0.715 \text{ eV}, & \text{CMB PLANCK [31]} \\ 0.170 \text{ eV}, & \text{CMB PLANCK+BAO [30]} : \\ 3.3 \text{ eV}, & \text{Weak lensing-only [32]} \end{cases} \quad (26)$$

where a lower limit could be provided by the neutrino oscillation measurements.

In order to extract the new physics effects, first we investigate the influence of ΔS_{31}^2 and $\sin 2\theta_3$ on $\sum_i m_{\nu_i}$ by imposing the experimental results on Δm_{Atm}^2 , Δm_{Sol}^2 and constraint given in Eq. (26) into Eq. (25). Contour plots in the parameter space $(\Delta S_{31}^2, \sin 2\theta_3)$ for fixed values of $\sum m_\nu$ (solid lines) and $m_{\bar{\nu}_e}$ probed in tritium β decay (dotted lines) are presented in Fig. 1, where a lower limit for the sum of the neutrino masses, $\sum_{i=1}^3 m_{\nu_i} \gtrsim 0.06 \text{ eV}$ could be provided by the neutrino oscillation measurements; upper limits 0.715 eV and 3.3 eV at 95% CL are given by Planck Collaboration [30] and weak lensing-only [32], respectively, in Eq. (26). In the plot⁷ we consider only eV-mass scale of sterile neutrino since too heavy neutrino is conflict with cosmology $\Delta N_\nu^{\text{eff}} < 0.2$ at 95% CL [36, 38].

The existence of sterile neutrino with the eV mass can also be constrained by β -decay experiments [33] and by $0\nu\beta\beta$ decay experiments [34]. The two types of mass ordering, discussed above, should be compatible with the existing constraints on the absolute scale of neutrino masses. The most sensitive experiment to search for the new physics effects in β -decay is to use the tritium decay process ${}^3\text{H} \rightarrow {}^3\text{He} + e^- + \bar{\nu}_e$. Non-zero neutrino masses distort the measurable spectrum of the emitted electron. The most stringent upper bounds on the $\bar{\nu}_e$ mass, $m_{\bar{\nu}_e}$, have been obtained from direct searches in the Mainz [39] and

⁷ The SBL anomalies including MiniBooNE data may indicate the existence of eV-mass sterile neutrino if those are interpreted as new oscillation effects, while present cosmological data coming from CMB + large-scale structure and big bang nucleosynthesis (BBN) do not prefer extra fully thermalized sterile neutrinos in the eV-mass range since they violate the hot dark matter limit on the neutrino mass [35]. The amount of thermalisation $\Delta N_\nu^{\text{eff}}$ as a function of neutrino parameters (mass splitting, mixing, and initial lepton asymmetry) has been quantitatively derived in Ref. [36], implying that the parameter space of $(\Delta m_3^2, \theta_3)$ responsible for the existence of an eV-mass sterile neutrino is allowed by requiring such sterile neutrino does not or partially equilibrium at the BBN epoch when the initial lepton asymmetry is large [36, 37].

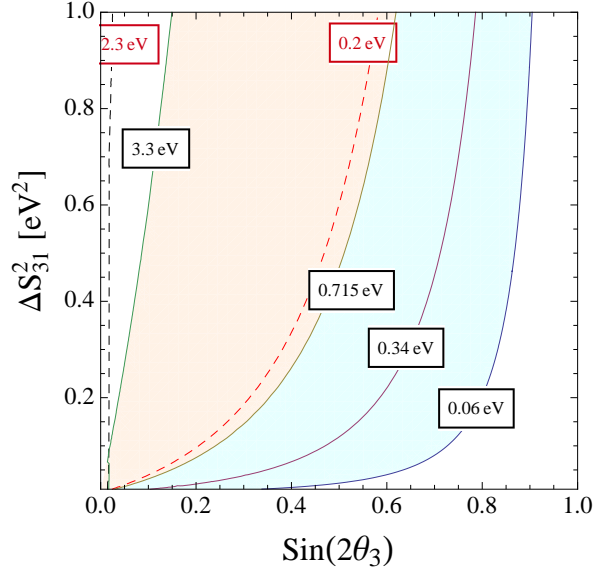


FIG. 1: Contour plots in the parameter space $(\Delta S_{31}^2, \sin 2\theta_3)$ for fixed values of $\sum_{i=1,2,3} m_\nu$ (solid lines) and $m_{\bar{\nu}_e}$ probed in tritium β decay (dotted lines). The black-dotted line corresponds to the upper bound $m_{\bar{\nu}_e} < 2.3$ eV [39], whereas the red-dotted line to a future sensitivity of $m_{\bar{\nu}_e} \lesssim 0.20$ [41]. For $\sum_{i=1,2,3} m_\nu$, we take the values from Eq.(26).

Troitsk [40] experiments at 95% CL:

$$m_{\bar{\nu}_e} = \left(\sum_{k=1}^3 |U_{ek}|^2 m_{\nu_k}^2 \right)^{\frac{1}{2}} < \begin{cases} 2.30 \text{ eV (Mainz)} \\ 2.05 \text{ eV (Troitsk)} \end{cases}. \quad (27)$$

In Fig. 1 the dotted lines show contour for the neutrino mass in tritium β decay $m_{\bar{\nu}_e}$ as a function of ΔS_{31}^2 and $\sin 2\theta_3$ with Eq. (19), where the black-dotted line corresponds to the upper bound $m_{\bar{\nu}_e} < 2.3$ eV [39], whereas the red-dotted line to a future sensitivity of $m_{\bar{\nu}_e} \lesssim 0.20$ [41]. As seen in Fig. 1, the cosmological bounds given in Eq. (26) are still tighter than the constraints from tritium β decay. The upcoming KATRIN experiment [41] planned to reach the sensitivity of $m_{\bar{\nu}_e} \sim 0.20$ eV will probe the region of the quasi-degenerate mass spectrum of the active neutrinos.

On the other hand, the $0\nu\beta\beta$ -decay rate [42] effectively measures the absolute value of the ee -component of the effective neutrino mass matrix \mathcal{M}_ν in Eq. (4). In the basis where the charged lepton mass matrix is real and diagonal, the $0\nu\beta\beta$ -decay rate can be expressed

as

$$(\mathcal{M}_\nu)_{ee} = \sum_{k=1}^3 W_\nu^* \begin{pmatrix} m_{\nu_k} I_3 & 0_3 \\ 0_3 & m_{s_k} I_3 \end{pmatrix} W_\nu^\dagger \Big|_{ee}. \quad (28)$$

Since the two mass eigenstates of first and second generations in each pseudo-Dirac pair have opposite CP parity, the third generation dominantly contributes to the $\beta\beta 0\nu$ -decay rate. For $||m_{\nu_3}| - |m_{s_3}|| \gg ||m_{\nu_k}| - |m_{s_k}||$ with $\theta_k \approx 0$ (for $k = 1, 2$), the $0\nu\beta\beta$ -decay rate, $m_{\beta\beta} \equiv |(\mathcal{M}_\nu)_{ee}|$, is approximately given by

$$m_{\beta\beta} \approx \frac{1}{2} \sin^2 \theta_{13} |(\sin 2\theta_3 + 1) |m_{\nu_3}| + (\sin 2\theta_3 - 1) |m_{s_3}||. \quad (29)$$

Using Eqs. (21) and (22) one can easily see that $\beta\beta 0\nu$ -decay rate becomes almost zero, $m_{\beta\beta} \approx 0$. Hence if the $\beta\beta 0\nu$ -decay rate is measured in near future the model would explicitly be excluded⁸.

IV. SHORT BASELINE NEUTRINO ANOMALIES

Now, let us study how our model can help to resolve the so-called short baseline neutrino anomalies in terms of neutrino oscillations. To see how the new sterile neutrino states cause such new oscillations at short-baselines with neutrino trajectory less than $1 < \text{km}$, let us bring out a conversion probability of new oscillations with the help of the neutrino mixing matrix Eq. (7). The conversion probability⁹ between the massive neutrinos that a neutrino eigenstate ν_a becomes eigenstate ν_b follows from the time evolution of mass eigenstates as

$$P_{\nu_a \rightarrow \nu_b}(W_\nu, L, E) = \left| (W_\nu^* e^{-i \frac{\mathcal{M}_\nu^2}{2E} L} W_\nu^T)_{ab} \right|^2, \quad (30)$$

⁸ Note that the claim of observation of $0\nu\beta\beta$ -decay of $^{76}_{32}\text{Ge}$ [43] is strongly disfavored by the recent results of the GERDA experiment [44].

⁹ The transition probability of $\nu_\alpha \rightarrow \nu_{s_i}$ between sterile and active neutrinos due to oscillations of active flavor ν_α (with $\alpha = e, \mu, \tau$) with sterile neutrinos ν_{s_i} (with $i = 1, 2, 3$), see Eq. (7), is given by $P_{\nu_\alpha \rightarrow \nu_{s_i}} \simeq \sum_{k=1}^2 U_{ik}^* U_{\alpha k} \tilde{U}_{\alpha k}^* \tilde{U}_{ik} \sin^2(\frac{\Delta m_{k1}^2}{4\pi} L) + U_{i3}^* U_{\alpha 3} \tilde{U}_{\alpha 3}^* \tilde{U}_{i3} \cos^2 2\theta_3 \sin^2(\frac{\Delta m_{k3}^2}{4\pi} L)$ where $\tilde{U} \equiv U_R$ in Eq. (7), $\Delta m_{kj}^2 \simeq m_{\nu_k}^2 - m_{\nu_j}^2$ and $\Delta S_{kj}^2 \simeq m_{s_k}^2 - m_{\nu_j}^2$ with $k > j = 1, 2, 3$ are used. For non-vanishing $\tilde{U}_{\mu 3}$, the new mass squared difference Δm_3^2 could be constrained by the probability of $\nu_\mu \rightarrow \nu_{s_i}$, while for tiny or vanishing $\tilde{U}_{\mu 3}$ one could not constrain the Δm_3^2 . In addition, the mass squared difference Δm_3^2 could be constrained by the disappearance of muon-type neutrinos and antineutrinos produced in the atmosphere, see Eq. (47) and Fig. 5, where the mixing θ_3 deviated from the maximal mixing $\pi/4$ is involved.

where $a, b = e, \mu, \tau, s_1, s_2, s_3$, L is the distance between the neutrino detector and the neutrino source, E is the neutrino energy, and $\hat{\mathcal{M}}_\nu \equiv W_\nu^T \mathcal{M}_\nu W_\nu$. We are interested in the flavor conversion between the active neutrinos ν_e, ν_μ, ν_τ satisfying the condition of Eq. (24) which leads to $\theta_{1(2)} \approx 0$. From Eq. (30) the flavor conversion probability between the three-active neutrinos can explicitly be expressed in terms of the oscillation parameters $\theta, \Delta m^2, L, E$, and mixing components $U_{\alpha i}$ of the 3×3 PMNS matrix as

$$\begin{aligned}
P_{\nu_\alpha \rightarrow \nu_\beta} = & \delta_{\alpha\beta} - \sum_{k=1}^2 |U_{\alpha k}|^2 |U_{\beta k}|^2 \sin^2 \left(\frac{\Delta m_k^2}{4E} L \right) - |U_{\alpha 3}|^2 |U_{\beta 3}|^2 \sin^2 \left(\frac{\Delta m_3^2}{4E} L \right) \cos^2 2\theta_3 \\
& - \sum_{k>j} \text{Re} [U_{\beta k}^* U_{\beta j} U_{\alpha j}^* U_{\alpha k}] \left[(1 + \delta_{k3} \sin 2\theta_3) \left\{ \sin^2 \left(\frac{\Delta m_{kj}^2}{4E} L \right) + \sin^2 \left(\frac{\Delta Q_{kj}^2}{4E} L \right) \right\} \right. \\
& \quad \left. + (1 - \delta_{k3} \sin 2\theta_3) \left\{ \sin^2 \left(\frac{\Delta S_{kj}^2}{4E} L \right) + \sin^2 \left(\frac{\Delta Q_{jk}^2}{4E} L \right) \right\} \right] \\
& + \frac{1}{2} \sum_{k>j} \text{Im} [U_{\beta k}^* U_{\beta j} U_{\alpha j}^* U_{\alpha k}] \left[(1 + \delta_{k3} \sin 2\theta_3) \left\{ \sin \left(\frac{\Delta m_{kj}^2}{2E} L \right) + \sin \left(\frac{\Delta Q_{kj}^2}{2E} L \right) \right\} \right. \\
& \quad \left. + (1 - \delta_{k3} \sin 2\theta_3) \left\{ \sin \left(\frac{\Delta S_{kj}^2}{2E} L \right) - \sin \left(\frac{\Delta Q_{jk}^2}{2E} L \right) \right\} \right], \quad (31)
\end{aligned}$$

where $\Delta Q_{kj}^2 \equiv m_{\nu_k}^2 - m_{\nu_j}^2$, and $\delta_{k3} = 1$ for $k = 3$ and 0 for $k \neq 3$. In the model the mixing parameters θ and Δm^2 are determined by nature, so experiments should choose L and E to be sensitive to oscillations through a given Δm^2 . As expected, in the limit of $m_{s_i} \rightarrow m_{\nu_i}$ and $\theta_i \rightarrow 0$ ($i = 1, 2, 3$), $P_{\nu_\alpha \rightarrow \nu_\beta}$ becomes the standard form of conversion probability for three active neutrinos in vacuum, as shown in Ref. [22]. The model has interesting features listed below under the assumption of CPT invariance:

- From Eq. (31), we see that $P_{\nu_\alpha \rightarrow \nu_\alpha} + P_{\nu_\alpha \rightarrow \nu_\beta} + P_{\nu_\omega \rightarrow \nu_\alpha} \leq 1$ with $\alpha \neq \beta \neq \omega = e, \mu, \tau$, whereas the probabilities for the standard three-active neutrino oscillations satisfy the relation $P_{\nu_\alpha \rightarrow \nu_\alpha} + P_{\nu_\alpha \rightarrow \nu_\beta} + P_{\nu_\omega \rightarrow \nu_\alpha} = 1$.
- The new oscillation effects attributed to Δm_i^2 , ΔS_{3k}^2 and ΔQ_{k3}^2 with $i = 1, 2, 3$ and $k = 1, 2$ in Eq. (31) can be maximum in the limit of $\theta_3 \rightarrow \pi/2$ (favored by the DNO and DIO), which can be relevant to short baseline neutrino experiments.
- In the limit of $\theta_3 \rightarrow \pi/4$ (favored by the IH, see Eq. (25)), the oscillatory term involving Δm_k^2 (with $k = 1, 2$) in Eq. (31) can give new oscillation effects only applicable to ABL oscillations. And thus, it is expected that this case could not provide a solution to the SBL anomalies.

To investigate the effects of new oscillations due to the new sterile neutrinos, we present approximated forms of neutrino oscillation probability based on the formula given by Eq. (31), which are relevant to interpreting short baseline neutrino anomalies. At a distance satisfying $L \ll 4\pi E/\Delta m_{\text{Sol}}^2, 4\pi E/\Delta m_{1(2)}^2$, the survival probability for $\bar{\nu}_e$ is approximated as

$$P_{\bar{\nu}_e \rightarrow \bar{\nu}_e} \approx 1 - \sin^4 \theta_{13} \sin^2 \left(\frac{\Delta m_{31}^2}{4E_{\bar{\nu}_e}} L \right) \cos^2 2\theta_3 - \frac{1}{2} \sin^2 2\theta_{13} \left[(1 - \sin 2\theta_3) \sin^2 \left(\frac{\Delta S_{31}^2}{4E_{\bar{\nu}_e}} L \right) + (1 + \sin 2\theta_3) \sin^2 \left(\frac{\Delta m_{31}^2}{4E_{\bar{\nu}_e}} L \right) \right]. \quad (32)$$

We note that new oscillatory terms vanish in the limit of $\theta_3 = \pi/4$, whereas they can reach maximum in the limit of $\theta_3 = \pi/2$. In the limit that $\frac{\Delta m_{31}^2}{4E_{\bar{\nu}_e}} L$ is negligible, but $\frac{4E_{\bar{\nu}_e}}{\Delta S_{31}^2} \simeq -\frac{4E_{\bar{\nu}_e}}{\Delta m_{31}^2} \sim L$, the ν_e disappearance probability $P_{\bar{\nu}_e \rightarrow \bar{\nu}_e}$ becomes

$$P_{\bar{\nu}_e \rightarrow \bar{\nu}_e} \approx 1 - \left[\sin^4 \theta_{13} \cos^2 2\theta_3 + \frac{1}{2} \sin^2 2\theta_{13} (1 - \sin 2\theta_3) \right] \sin^2 \left(\frac{\Delta S_{31}^2}{4E_{\bar{\nu}_e}} L \right). \quad (33)$$

Similarly, the probabilities $P_{\bar{\nu}_\mu \rightarrow \bar{\nu}_e}$ and $P_{\bar{\nu}_\mu \rightarrow \bar{\nu}_\mu}$ are approximately given by

$$P_{\bar{\nu}_\mu \rightarrow \bar{\nu}_e} \approx \frac{1}{4} \sin^2 2\theta_{13} \sin^2 \theta_{23} [2 - 2 \sin 2\theta_3 - \cos^2 2\theta_3] \sin^2 \left(\frac{\Delta S_{31}^2}{4E_{\bar{\nu}_e}} L \right), \quad (34)$$

$$P_{\bar{\nu}_\mu \rightarrow \bar{\nu}_\mu} \approx 1 - \sin^2 \theta_{23} \cos^2 \theta_{13} \left[\sin^2 \theta_{23} \cos^2 \theta_{13} (\cos^2 2\theta_3 - 2 \sin 2\theta_3 + 2) - 2(1 - \sin 2\theta_3) \right] \sin^2 \left(\frac{\Delta S_{31}^2}{4E} L \right), \quad (35)$$

The above formulae for the probabilities can be applied to not only the experimental data from LSND and MiniBooNE but also the reactor neutrino flux anomaly. The expressions Eqs. (33,34,35) can be compared with those in the 3+1 model [20, 21] given by

$$P_{\bar{\nu}_\alpha \rightarrow \bar{\nu}_\beta}^{3+1} \simeq \sin^2 2\theta_{\alpha\beta} \sin^2 \left(\frac{\Delta m_{41}^2 L}{4E} \right), \quad P_{\bar{\nu}_\alpha \rightarrow \bar{\nu}_\alpha}^{3+1} \simeq 1 - \sin^2 2\theta_{\alpha\alpha} \sin^2 \left(\frac{\Delta m_{41}^2 L}{4E} \right), \quad (36)$$

where $\alpha, \beta = e, \mu, \tau, s$. The oscillation amplitudes depend only on the absolute values of the elements in the forth column of the mixing matrix in the 3 + 1 model,

$$\sin^2 2\theta_{\alpha\beta} = 4|U_{\alpha 4}|^2 |U_{\beta 4}|^2, \quad (\alpha \neq \beta), \quad \sin^2 2\theta_{\alpha\alpha} = 4|U_{\alpha 4}|^2 (1 - |U_{\alpha 4}|^2). \quad (37)$$

Then, ΔS_{31}^2 plays the same role of Δm_{41}^2 in (36), and $\sin^2 2\theta_{\alpha\beta}$ and $\sin^2 2\theta_{\alpha\alpha}$ correspond to the parameters multiplied in front of oscillatory terms in Eqs. (33,34,35).

On the other hand, for the baselines optimized by the oscillation parameters $\Delta m_{31}^2 \sim 2.5 \times 10^{-3} \text{ eV}^2$ and $E_{\bar{\nu}_e} \sim \text{MeV}$, *i.e.* $4\pi E/\Delta S_{31}^2 \ll L \ll 4\pi E/\Delta m_{\text{Sol}}^2, 4\pi E/\Delta m_{1(2)}^2$, the

antineutrino probability in Eq. (33) is approximately given by

$$P_{\bar{\nu}_e \rightarrow \bar{\nu}_e} \approx 1 - \frac{1}{2} \sin^4 \theta_{13} \cos^2 2\theta_3 - \frac{1}{2} \sin^2 2\theta_{13} \left[\frac{1 - \sin 2\theta_3}{2} + (1 + \sin 2\theta_3) \sin^2 \left(\frac{\Delta m_{31}^2}{4E_{\bar{\nu}_e}} L \right) \right] \quad (38)$$

where the terms including ΔS_{31}^2 are averaged out.

Now, let us examine how the SBL anomalies can be resolved or alleviated by the formulae given above. Note that all plots in what follows are based on the exact formulae in Eq. (31) and for comparison we use the best-fit values of NO in Eq. (20) unless otherwise noted.

A. New Interpretation of Reactor Neutrino Results

In order to probe the effects of the new sterile neutrino from the experimental results obtained at the reactor neutrino experiments, Daya Bay, RENO and Double Chooze (see Ref. [45]), we interpret them in terms of neutrino oscillations including the new sterile neutrino by using the new reactor antineutrino probability in Eq. (38). Adopting Δm_{31}^2 by the values determined from atmospheric neutrino oscillation, we can obtain new values of θ_{13} along with θ_3 by equating Eq. (38) with the value of $\bar{\nu}_e$ survival probability for the three-active neutrino oscillation given by

$$P_{3\nu}(\bar{\nu}_e \rightarrow \bar{\nu}_e) \approx 1 - \sin^2 2\theta_{13} \sin^2 \left(\frac{\Delta m_{31}^2}{4E_{\bar{\nu}_e}} L \right) = 0.914_{-0.009}^{+0.009}, \quad (39)$$

where the numerical result is obtained by taking $L = 1.8 \text{ km}$, $E_{\bar{\nu}_e} = 3.5 \text{ MeV}$, $\Delta m_{31}^2 = 2.5 \times 10^{-3} \text{ eV}^2$, and at 3σ $\theta_{13} [^\circ] = 8.45_{-0.45}^{+0.45}$ given in Eq. (20). Then, θ_{13} becomes a function of θ_3 . In the right panel of Fig. 2, each depth of sinusoidal curves is proportional to $\sin^2 2\theta_{13}$ as indicated in Eq. (38). The left panel of Fig. 2 shows the behavior of θ_{13} driven by Eq. (38) as a function of θ_3 , where the values of θ_{13} are enhanced by around 6% at $\theta_3 = 1.28$ and 13% at $\theta_3 = 1.50$ (recalling that the value of $\theta_3 \lesssim 1.28$ for $\Delta S_{31}^2 = 0.6 \text{ eV}^2$ is constrained by cosmological data¹⁰, see Fig. 1):

$$\theta_{13} [^\circ] = 8.96_{-0.49}^{+0.45} \text{ at } \theta_3 = 1.28 [\text{rad}]; \quad \theta_{13} [^\circ] = 9.54_{-0.53}^{+0.49} \text{ at } \theta_3 = 1.50 [\text{rad}]. \quad (40)$$

In the right panel of Fig. 2, we fix $E_{\bar{\nu}_e} = 3.5 \text{ MeV}$ and $\Delta S_{31}^2 = 0.6 \text{ eV}^2$ and the cyan and red plots correspond to the cases of $(\theta_3, \theta_{13}) = (1.28, 0.156)$ and $(1.50, 0.167)$, respectively.

¹⁰ If the sum of active neutrino masses constrained by PLANCK data in Eq. (26) is relaxed making the value of θ_3 large *i.e.* $\theta_3 > 1.28$, the value of θ_{13} can also be enhanced and in turn the LSND/MiniBooNE anomaly could be explained as seen in the following section.

Note that the value of θ_{13} corresponds to the central value evaluated at the given value of θ_3 with the new oscillation formula Eq. (38), and the red-triangle, red-square (black-square), blue-circle, black-star, and black-circle error bars represent the values of the parameter R defined by the ratio of reactor antineutrino flux to the theoretical prediction obtained from the RENO [45], Double Chooz [45, 46], Daya Bay [47], Palo Verde [48], and Chooz [49], where the error bars represent the experimental uncertainties. The values of R from RENO, Double Chooz, Daya Bay, Palo Verde, and Chooz have been obtained by subtracting the effects of θ_{13} -driven oscillations. And the yellow band stands for the world average of R updated after including Daya Bay result $R = 0.945 \pm 0.007(\text{exp.})$ [47], compared with the past global average $R_{\text{past}} = 0.927$ [21] indicated as black-dashed horizontal line, where the uncertainty of common reactor model is ± 0.023 with respect to the Huber-Mueller model.

B. Reactor Neutrino Flux Anomaly

The reactor antineutrino anomaly [9] is the experimental result presenting a deficit of the rate of $\bar{\nu}_e$ in several SBL reactor neutrino experiments with $L \sim (10 - 100)$ m and $E_{\bar{\nu}_e} \sim \text{MeV}$. In reactor neutrino experiments, electron antineutrinos are detected through the inverse neutron decay process $\bar{\nu}_e + p \rightarrow n + e^+$ in liquid-scintillator detectors. To interpret the deficit of observed reactor neutrino fluxes relative to the prediction (Huber-Mueller model [50]) in terms of neutrino oscillation including the new sterile neutrinos, it is relevant to use the probability given by Eq. (33). We note that the reactor neutrino flux anomaly is not clearly explained at $L \lesssim 500$ m as in the 3+1 model [20, 21]: Eq. (33) clearly depends on the electron antineutrino energy $E_{\bar{\nu}_e}$ and its flight length L , and the nature of sterile neutrino associated with ΔS_{31}^2 and θ_3 . Once experimental inputs L and $E_{\bar{\nu}_e}$ are fixed the allowed regions of ΔS_{31}^2 and θ_3 can be obtained from $P_{\bar{\nu}_e \rightarrow \bar{\nu}_e}$ in Eq. (33), constraints by $\sum m_\nu$ in Eq. (26), and $m_{\bar{\nu}_e}$ in Eq. (27) as shown in Fig. 1. Note that the values of the model parameters θ_3 and ΔS_{31}^2 favored by the Planck data in Eq. (26) are not conflict with the NEOS ($L = 24$ m) and DANSS ($L = 10.7 \rightarrow 12.7$ m) results [51]¹¹.

¹¹ The recent NEOS and DANSS results [51] have a tension with the Gallium and reactor anomalies in the 3+1 model [21], while their results show a preference on our model predictions.

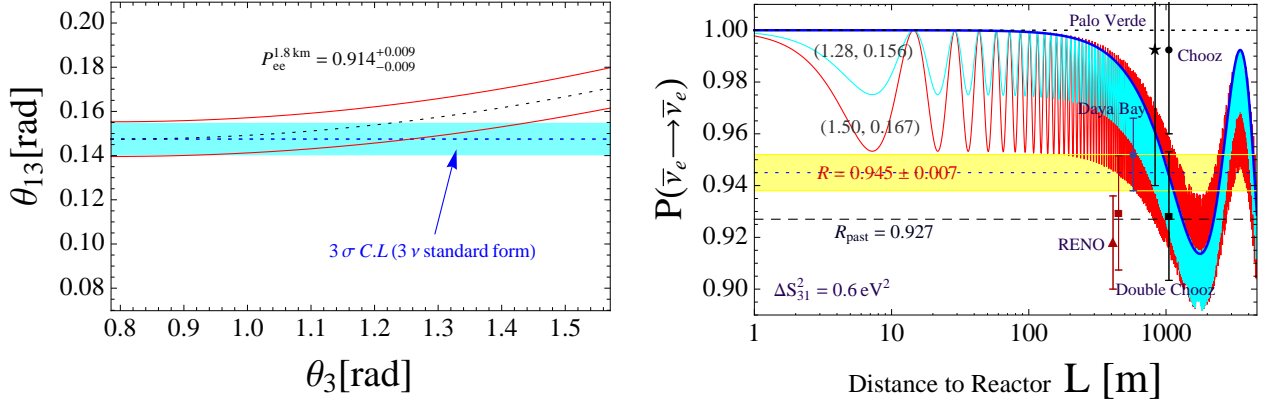


FIG. 2: Left plot represents θ_{13} vs. $\sin(2\theta_3)$, where the cyan band(horizontal dotted-line) stands for $\theta_{13}[\circ] = 8.45^{+0.45}_{-0.45}$ at 3σ (best-fit value)given in Eq. (20). Right plot represents $P_{\bar{\nu}_e \rightarrow \bar{\nu}_e}$ vs. L [meters] for $E_{\bar{\nu}_e} = 3.5$ MeV where the standard form of $P_{3\nu}(\bar{\nu}_e \rightarrow \bar{\nu}_e)$ for a fixed $\theta_{13} = 8.45^\circ$ is plotted by the blue-solid curve, and the red and cyan-sine curves are obtained from the exact $P_{\bar{\nu}_e \rightarrow \bar{\nu}_e}$ for $(\theta_3, \theta_{13}) = (1.50, 0.167)$ and $(1.28, 0.156)$ with $\Delta S_{31}^2 = 0.6 \text{ eV}^2$. Error bars represent recent several measurements of R , where the yellow band stands for the most recent world average [47] and the black-dashed horizontal line for the previous world average [21].

C. LSND anomaly and MiniBooNE data

The LSND experiment [12] reported observation of a statistically suggestive excess of $\bar{\nu}_e$ events in a beam of $\bar{\nu}_\mu$ produced by μ^+ decay at rest, $\mu^+ \rightarrow e^+ + \nu_e + \bar{\nu}_\mu$ with 3.8σ significance¹². The MiniBooNE experiments also observed ν_e and $\bar{\nu}_e$ appearance in ν_μ and $\bar{\nu}_\mu$ beams, respectively having the same L/E as in LSND [13]. In the left panel of Fig. 3, the black error bars stand for the LSND [12] data and the blue (red) error bars stand for the MiniBooNE data excess in (anti-)neutrino mode, at the baseline 541 m from the beryllium target, in particular, in the interval of energies $200 < E_\nu < 475$ MeV, which corresponds to L/E range beyond that probed in the LSND experiment [13]. It has been shown that the observed excesses in MiniBooNE experiment are in agreement with the LSND result, and provide a good fit to a large Δm^2 solution in a two-neutrino oscillation framework, even though the two experiments have completely different neutrino energies, neutrino fluxes,

¹² The similar KARMEN collaboration [52] did not measure any excess of $\bar{\nu}_e$ events over the background at a mean distance $L \simeq 17.7$ m with $E_{\bar{\nu}_\mu} = 12 \sim 52.8$ MeV, which did not fully exclude the LSND result.

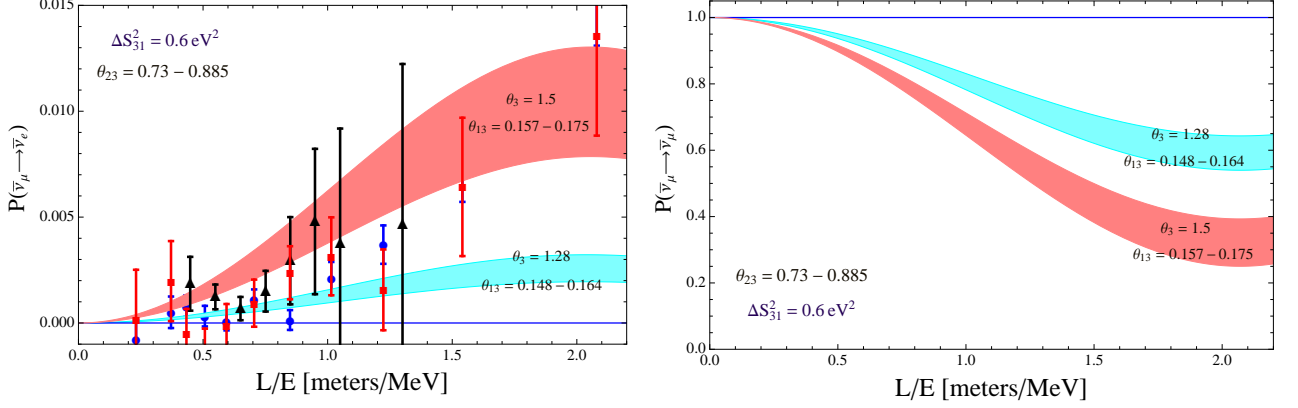


FIG. 3: Plots of $P_{\bar{\nu}_\mu \rightarrow \bar{\nu}_e}$ (left) and $P_{\bar{\nu}_\mu \rightarrow \bar{\nu}_\mu}$ (right) *vs.* L/E [m/MeV]. In the left panel data points with blue(red)-bar correspond to neutrino (antineutrino) mode in MiniBooNE [13] and those with black-bar to the LSND [12] data. The horizontal-blue lines stand for the standard form of probability for $\bar{\nu}_e$ appearance (left) and $\bar{\nu}_\mu$ disappearance (right), while the red- and cyan-band curves represent the new conversion probabilities in Eq. (31) for the sum of active neutrino mass $\sum m_\nu = 2.673$ and 0.705 eV, respectively. The band width is due to the uncertainty of $\theta_{23} = 41.8 \sim 50.7^\circ$ and the new ranges of θ_{13} in Eq. (40).

reconstruction, backgrounds, and systematic uncertainties.

The LSND and MiniBooNE excesses could be explained by $\bar{\nu}_\mu \rightarrow \bar{\nu}_e$ oscillation whose probability is given by Eq. (34). As in the case of $3 + 1$ model [20, 21], to explain the excess of $\bar{\nu}_e$ events, we need $\Delta S_{31}^2 \sim O(1) \text{eV}^2$ and large values of $\theta_3 (> \pi/4)$. In particular, when $\theta_3 \rightarrow \pi/2$ favored by the degenerate case (DNO and DIO), $P_{\bar{\nu}_\mu \rightarrow \bar{\nu}_e} \simeq \frac{1}{4} \sin^2 2\theta_{13} \sin^2 \theta_{23} \sin^2 \left(\frac{\Delta S_{31}^2 L}{4E_{\bar{\nu}_e}} \right) \lesssim 0.012$ for the LSND and MinibooNE experiments. But this case leads to a large value of the sum of three active neutrino masses, as shown in Fig. 3. The left panel of Fig. 3 presents plots of $P_{\bar{\nu}_\mu \rightarrow \bar{\nu}_e}$ versus L/E (m/MeV) for two benchmark points of $\theta_3 = 1.5$ and 1.28 for a given $\Delta S_{31}^2 = 0.6 \text{eV}^2$. In the numerical estimation, we vary the parameter space $(\theta_{13}, \theta_{23})$ in the ranges of $(0.157 - 0.175, 0.730 - 0.885)$ and $(0.148 - 0.164, 0.730 - 0.885)$ which correspond to $\sum_{i=e,\mu,\tau} m_{\nu_i} = 2.673$ and 0.705 eV, respectively, for two benchmark points. It is worthwhile to note that the parameter space of $(\Delta S_{31}^2, \theta_3)$, as presented in Fig. 1, is constrained through $\sum_{i=e,\mu,\tau} m_{\nu_i}$ by the cosmological data and the effective neutrino mass in tritium β -decay. However, statistical uncertainties have to be reduced by gaining more data in order to confirm our model in the following two respects: (i) the two data points in the left panel of Fig. 3 from MiniBooNE at $L/E \gtrsim 1.5$

(m/MeV) seem to favor $\sum m_\nu \gtrsim 0.705$ eV, which is disfavored by Planck Collaboration (TT+lowP) at 95% CL [31] while still not excluded by the weak lensing only data [32], (ii) it seems that the ν_e (blue-bars) and $\bar{\nu}_e$ (red-bars) modes in MiniBooNE data, in principle, could be discriminated by considering the CP violating term in Eq. (31). In the model setup, however, it seems not possible to discriminate between them within the short baseline due to the CP violating terms proportional to $-4\sin(\Delta m_{21}^2 L/2E)$.

In addition, searching for the $\bar{\nu}_e$ appearance in LSND and MiniBooNE also implies $\bar{\nu}_\mu$ disappearance whose oscillation probability is given by Eq. (35). In the right panel of Fig. 3, we present how the survival probability $P_{\bar{\nu}_\mu \rightarrow \bar{\nu}_\mu}$ behaves along with L/E (m/MeV) for the same cases in the left panel of Fig. 3. The large deviation from $P_{\bar{\nu}_\mu \rightarrow \bar{\nu}_\mu} = 1$ at large L/E as shown in the right panel of Fig. 3 is the characteristic feature of this model we consider, which makes our model different from $3 + 1$ model. Accelerator based experiments for $\bar{\nu}_\mu$ (or ν_μ) disappearance, such as MINOS and MINOS+ neutrino experiments [53], may be sensitive to oscillations involving sterile neutrinos [54] for the regions of $10^{-2} \lesssim L/E$ (km/GeV) $\lesssim 0.75$ at near detector ($L = 1.04$ km) and $8 \lesssim L/E$ (km/GeV) $\lesssim 7 \times 10^2$ at far detector ($L = 735$ km). The former region can cover L/E values of order 1m/MeV in the right panel of Fig. 3, while the latter can cover range of $L/E \sim \mathcal{O}(10 \sim 100)$ [km/GeV], comparing with the results of the atmospheric muon neutrino events observed¹³ in Super-Kamiokande [57] and the left plot in Fig. 5. To see such an oscillation dip due to new sterile neutrino as shown in the right panel of Fig. 3, we need the neutrino baseline ~ 6 km (14 km) for detector having ~ 3 GeV (7 GeV) peak energy with $\Delta S_{31}^2 = 0.6 \text{ eV}^2$.

In addition, such ν_μ disappearance oscillation effect could be observed at $L/E \sim 1.2$ [m/MeV] with $E_{\nu_\mu} \sim 0.5$ GeV and $L = 600$ m in the Short-Baseline Neutrino (SBN) Program experiment [58] for the same model parameters in Fig. 3. And, at the far detector ($L = 735$ km) a possibility on searching for signatures of sterile neutrinos in the ν_μ disappearance by using Eq. (35) will be considered in section V B.

¹³ The recent results from the MINOS and MINOS+ far detector data in Neutrino 2018 [45] including the result of IceCube DeepCore [55] seem to be in agreement with the expected in the three neutrino standard form in the range $20 \lesssim L/E$ [km/GeV] $\lesssim 2000$, while in their past results [54, 56] there are some large deficit data points which seem to be in agreement with the oscillating signatures of light sterile neutrinos, see the cyan-curve in the left panel of Fig. 5.

D. Earth matter effects

Let us explore the Earth matter effect [27, 59] by examining the propagation of atmospheric neutrinos produced in cosmic-ray air showers from the Earth's atmosphere to the inside of the Earth. When muon neutrinos pass through the Earth matter, the MSW effect [27] should be taken into account. Path-length ranges from 10 km to 1.27×10^4 km depending on arrival zenith angle. The matter density encountered by neutrinos propagating is on average $\rho_{\oplus} \sim 3 \text{ g/cm}^3$ in the Earth's crust and outer mantle, $\sim 5 \text{ g/cm}^3$ in the inner mantle, and between 10 and $\sim 13 \text{ g/cm}^3$ in the core [60]. Muon neutrino oscillations modified due to matter effects can produce distinctive signatures of sterile neutrinos in the large set of high energy atmospheric neutrino data (both in the TeV energy window from IceCube [61] and at lower energy from DeepCore [55]). For $E_{\nu} > 100 \text{ GeV}$, three-active neutrino oscillation length larger than the diameter of the Earth and can be neglected. In order to find appropriate physics parameters ($\theta, \Delta m^2, L, E$) for atmospheric neutrino oscillations, we consider the effective Hamiltonian in-matter \mathcal{H}^m in flavor basis, which has the form of 6×6 matrix

$$\mathcal{H}^m = \frac{1}{2E_m} \left[W_{\nu}^* \begin{pmatrix} m_{\nu_k}^2 I_3 & 0_3 \\ 0_3 & m_{s_k}^2 I_3 \end{pmatrix} W_{\nu}^T + \begin{pmatrix} A_{\alpha} I_3 & 0_3 \\ 0_3 & 0_3 \end{pmatrix} \right], \quad (41)$$

where $k = 1, 2, 3$ and $\alpha = e, \mu, \tau$. Here the parameters $A_{\alpha} = 2E_m V_{\alpha}$ is a measure of the importance of matter effect with the matter-induced effective potential; V_e, V_{μ}, V_{τ} , and $V_s = 0$ are the potentials experienced by the electron, muon, tau, and sterile neutrinos respectively, and E_m is the neutrino energy in matter. For anti-neutrinos $V_{\alpha} \rightarrow -V_{\alpha}$. ν_e 's have charged-current (CC) interactions with electrons and neutral-current (NC) interactions with electrons and nucleons, $V_e = \sqrt{2}G_F(N_e - N_n/2)$, while ν_{μ} 's and ν_{τ} 's have only NC interactions, $V_{\mu} = V_{\tau} = \sqrt{2}G_F(-N_n/2)$, and any ν_s 's have no interactions, $V_s = 0$, where Fermi's constant, G_F , and the average electron and neutron densities along the neutrino path, N_e and N_n , respectively.

The mass matrix of the massive neutrinos in matter can be diagonalized through a new unitary mixing matrix W_m ,

$$W_m = \begin{pmatrix} U_L & 0_3 \\ 0_3 & U_R \end{pmatrix} \begin{pmatrix} V_1 & iV_1 \\ V_2 & -iV_2 \end{pmatrix} \begin{pmatrix} e^{i\phi_k} \cos \theta_k^m I_3 & -e^{i\phi_k} \sin \theta_k^m I_3 \\ e^{-i\phi_k} \sin \theta_k^m I_3 & e^{-i\phi_k} \cos \theta_k^m I_3 \end{pmatrix}. \quad (42)$$

The diagonalization of \mathcal{H}^m by the unitary matrix W_m in matter gives a condition

$$A_\alpha |U_{\alpha k}|^2 = \Delta m_k^2 \frac{\sin 2(\theta_k^m - \theta_k)}{\cos 2\theta_k^m}, \quad (43)$$

and its effective mass-squared eigenvalues in matter which are positive

$$\begin{aligned} \tilde{m}_{\nu_k}^2 &= (m_{\nu_k}^2 + m_{s_k}^2) \cos^2(\theta_k^m - \theta_k) - m_{s_k}^2 \cos 2(\theta_k^m - \theta_k) + \frac{\Delta m_k^2}{2} \frac{\sin 2(\theta_k^m - \theta_k)}{\cos 2\theta_k^m} (1 + \sin 2\theta_k^m) \\ \tilde{m}_{s_k}^2 &= (m_{\nu_k}^2 + m_{s_k}^2) \cos^2(\theta_k^m - \theta_k) - m_{\nu_k}^2 \cos 2(\theta_k^m - \theta_k) + \frac{\Delta m_k^2}{2} \frac{\sin 2(\theta_k^m - \theta_k)}{\cos 2\theta_k^m} (1 - \sin 2\theta_k^m) \end{aligned} \quad (44)$$

For $\theta_{1(2)} \sim 0$ corresponding to $\Delta m_{1(2)}^2 < 10^{-12} \text{ eV}^2$ in Eq. (24) we assume no Earth mat-

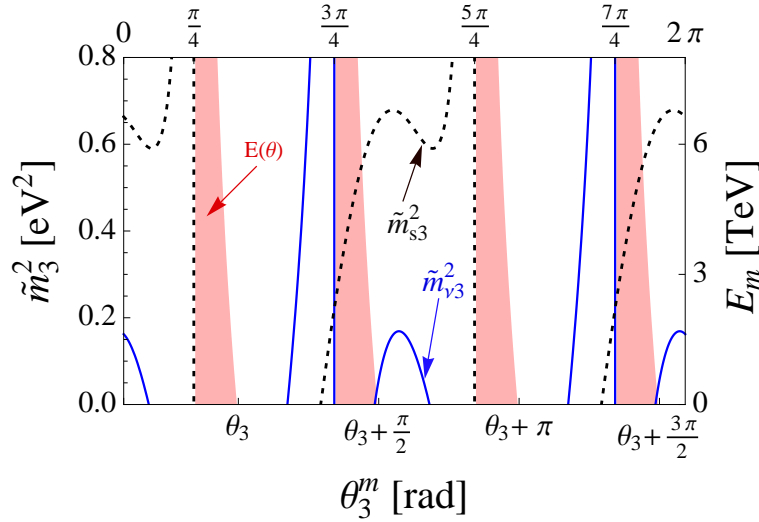


FIG. 4: Plots of the effective mass-squared $\tilde{m}_{s_3}^2$ (black-dotted curves) and $\tilde{m}_{\nu_3}^2$ (blue-solid curves) in Eq. (44) and the effective energy $E(\theta) \equiv E_m(\theta_3^m)$ in Eq. (45) as a function of θ_3^m . The shaded regions stand for the allowed parameter space by the matter effect, while the white regions for vacuum-like oscillations.

ter effects occurs, leading to $\theta_k^m \rightarrow \theta_k$. Then from Eq. (43) the energy of upward-going atmospheric muon neutrinos in matter can be derived as

$$E_m \simeq \frac{1.6 \text{ TeV}}{\sin^2 \theta_{23} \cos^2 \theta_{13}} \left(\frac{\Delta m_3^2}{-0.6 \text{ eV}^2} \right) \left(\frac{5 \text{ g/cm}^3}{\rho_\oplus} \right) \frac{\sin 2(\theta_3^m - \theta_3)}{\cos 2\theta_3^m}, \quad (45)$$

and $\sin 2(\theta_3^m - \theta_3) \rightarrow \sin 2(\theta_3 - \theta_3^m)$ for $\bar{\nu}_\mu$, indicating that the energy E_m varies with the matter mixing angle θ_3^m . Note that as $\theta_3^m \rightarrow \theta_3 + n\pi/2$ (with $n = 0, 1, 2, 3, \dots$), the matter effect gets faded. In Fig. 4 we plot the effective mass-squared $\tilde{m}_{s_3}^2$ (black-dotted lines), $\tilde{m}_{\nu_3}^2$ (blue-solid lines) and E_m (red-bands) in terms of θ_3^m . Thanks to the positiveness of $\tilde{m}_{s_3}^2$,

$\tilde{m}_{\nu_3}^2$ and E_m , they are predicted for limited regions of θ_3^m as can be seen in Fig. 4. The lines overlapped with the red bands represent the effective masses affected by Earth matter effect. In the limit of $E_m \rightarrow 0$, $\tilde{m}_{\nu_3}^2$ approaches $m_{\nu_3}^2$, implying that the matter effect becomes negligible for muon neutrinos with energies $\gg 1$ GeV passing through the interior of Earth. Hence, it is expected that the ν_μ (or $\bar{\nu}_\mu$) disappearance probability for high energy ($\gg 1$ GeV) muon neutrinos passing through the Earth interior to search for the oscillation signatures of light sterile neutrinos is the same as the one in vacuum-like derived in Eq. (30).

Recently, the high-energy IceCube detector has measured the atmospheric muon neutrino spectrum at energy $E_{\nu_\mu} = 320 \text{ GeV} \sim 20 \text{ TeV}$ in hope of finding the oscillation signatures of light sterile neutrinos [61], but no evidence for anomalous ν_μ or $\bar{\nu}_\mu$ disappearance is observed. The results coincide with the model prediction on the matter effects at the same energy window, contrary to the models in Refs. [62–67] which has a tension with ν_μ (or $\bar{\nu}_\mu$) disappearance experiments. And the IceCube sub-detector DeepCore at energy window of atmospheric muon neutrinos $10 \sim 100 \text{ GeV}$ [55] can also have potential to search for the signature of light sterile neutrinos as discussed in the next section.

V. NEW EFFECTS IN SOLAR AND ATMOSPHERIC OSCILLATIONS

Now, let us examine the oscillation effects due to the sterile neutrinos on the long baseline experiments such as KamLAND [22], T2K [68], MINOS and MINOS+ Collaboration [53], solar neutrino and atmospheric neutrino experiments [55, 57].

A. New effects in ν_e disappearance from KamLAND, T2K and Solar neutrino oscillation

For the long baseline such as KamLAND experiment [69], the survival probability of $\bar{\nu}_e$ events in the model we consider is approximately given by

$$P_{\bar{\nu}_e \rightarrow \bar{\nu}_e} \approx 1 - \frac{1}{2}(\sin^2 2\theta_{13} - \sin^4 \theta_{13} \cos^2 2\theta_3) - \cos^4 \theta_{13} \sin^2 2\theta_{12} \sin^2 \left(\frac{\Delta m_{21}^2}{4E} L \right) \quad (46)$$

where we assume CP invariance and the term $\sin^2 \left(\frac{\Delta m_{32}^2}{4E} L \right)$ is averaged out for long baseline (e.g. $\langle L \rangle \simeq 180 \text{ km}$). Applying Eq. (46) to KamLAND data [70], we can extract the value of θ_3 with precise measurements of Δm_{21}^2 and θ_{12} . However, we see that Eq. (46) is almost

the same as the expression for the standard oscillation probability for three-active neutrinos because the new term concerned with θ_3 is negligible due to the tiny value of $\sin^4 \theta_{13} \simeq 5 \times 10^{-4}$. Thus, new effects due to the sterile neutrinos on KamLAND, T2K experiments and solar neutrino oscillation are negligible.

Since the T2K experiment at the ND280 near detectors covers L/E values of order 1 m/MeV, an information such as θ_3 in Eq. (46) on sterile neutrinos can also be extracted. It has performed a search for ν_e disappearance in a neutrino beam whose ν_e component is peaked at an energy of 500 MeV [68]. From Eq. (46) in the limit $L \ll 4\pi E_{\nu_e}/\Delta m_{21}^2$ the ν_e disappearance probability driven by the sterile neutrino can easily be obtained for the baseline of 280 m, and it shows that its effect on sterile neutrino is negligible due to the tiny value of $\sin^4 \theta_{13}$.

B. New effects in ν_μ disappearance from SuserK and IceCube

In addition to the TeV muon neutrinos discussed in previous section, the IceCube Collaboration can also have potential to search for the signature of light sterile neutrinos by observing atmospheric neutrinos in the tens-of-GeV range through its sub-detector DeepCore (for reference, see Ref. [55]). The atmosphere of the Earth is constantly being bombarded by cosmic rays, primarily made up of protons and helium nuclei produced by atmospheric objects [22]. These cosmic rays have been observed over a wide range of energy, from 1 GeV to 10^{11} GeV. We recall atmospheric neutrinos with energy of \sim a few GeV which are mostly produced by primary cosmic rays with energy of \sim 100 GeV [22]. According to the three-active neutrino oscillation probability, large deficits of muon neutrino have been observed in upward-going events and at $L/E \sim 230$ km/GeV [22] as shown by blue sinusoidal curves in Fig. 5 which is well consistent with the Super-Kamiokande's atmospheric neutrino data [57]. For the baselines $L \ll 4\pi E/\Delta m_{\text{Sol}}^2, 4\pi E/\Delta m_{1(2)}^2$, which is relevant to the atmospheric neutrino, the survival and conversion probability of muon neutrino are approximately given

by

$$P_{\nu_\mu \rightarrow \nu_\mu} \approx 1 - \sin^4 \theta_{23} \cos^4 \theta_{13} \cos^2 2\theta_3 \sin^2 \left(\frac{\Delta m_3^2}{4E} L \right) - 2 \sin^2 \theta_{23} \cos^2 \theta_{13} (1 - \sin^2 \theta_{23} \cos^2 \theta_{13}) \\ \times \left[(1 + \sin 2\theta_3) \sin^2 \left(\frac{\Delta m_{31}^2}{4E} L \right) + (1 - \sin 2\theta_3) \sin^2 \left(\frac{\Delta S_{31}^2}{4E} L \right) \right], \quad (47)$$

$$P_{\nu_\mu \rightarrow \nu_\tau} \approx \frac{1}{2} \sin^2 2\theta_{23} \cos^4 \theta_{13} \left[-\frac{1}{2} \cos^2 2\theta_3 \sin^2 \left(\frac{\Delta m_3^2}{4E} L \right) \right. \\ \left. + (1 + \sin 2\theta_3) \sin^2 \left(\frac{\Delta m_{31}^2}{4E} L \right) + (1 - \sin 2\theta_3) \sin^2 \left(\frac{\Delta S_{31}^2}{4E} L \right) \right], \quad (48)$$

where $\Delta m_{3j}^2 \approx \Delta Q_{3j}^2$ and $\Delta S_{3j}^2 \approx |\Delta Q_{j3}^2|$ with $j = 1, 2$ are used. Since $L \gg 4\pi E / \Delta S_{31}^2$, $\sin^2 \left(\frac{\Delta S_{31}^2 (\Delta m_3^2)}{4E} L \right)$ is averaged out. As expected, the new oscillation probability for ν_μ (or $\bar{\nu}_\mu$) disappearance given in Eq.(47) can be sizably deviated depending on the parameters ΔS_{31}^2 , θ_3 from the three-active neutrino oscillation probability. From Eqs.(47) and (48), we easily see that $1 - P_{\nu_\mu \rightarrow \nu_\tau} - P_{\nu_\mu \rightarrow \nu_\mu} \geq P_{\nu_e \rightarrow \nu_\mu}$ in vacuum. At a distance $L \ll 4\pi E / \Delta m_{\text{Sol}}^2, 4\pi E / \Delta m_{1(2)}^2$, the probability $P_{\bar{\nu}_\mu \rightarrow \bar{\nu}_e} (= P_{\nu_e \rightarrow \nu_\mu})$ is given by

$$P_{\nu_e \rightarrow \nu_\mu} \approx \frac{1}{2} \sin^2 \theta_{23} \sin^2 2\theta_{13} \left[-\frac{1}{2} \cos^2 2\theta_3 \sin^2 \left(\frac{\Delta m_3^2}{4E} L \right) \right. \\ \left. + (1 + \sin 2\theta_3) \sin^2 \left(\frac{\Delta m_{31}^2}{4E} L \right) + (1 - \sin 2\theta_3) \sin^2 \left(\frac{\Delta S_{31}^2}{4E} L \right) \right]. \quad (49)$$

For $L \gg 4\pi E / \Delta S_{31}^2$, $\sin^2 \left(\frac{\Delta S_{31}^2}{4E} L \right)$ in Eq.(49) is averaged out.

The left panel of Fig.5 shows ν_μ survival probability as a function of L/E (km/GeV), where the blue sinusoidal curve and the cyan rapid oscillations stand for the probability predicted from the standard form of probability for three active neutrinos and that from the new oscillation probability with parameters $\theta_3 = 1.28$ and $\Delta S_{31}^2 = 0.6 \text{ eV}^2$, and the data points are atmospheric neutrino events observed in Super-Kamiokande [57]. As shown in the plot the atmospheric neutrino data from Super-Kamiokande [57] are well consistent with the new $\nu_\mu \leftrightarrow \nu_\tau$ oscillation (cyan curve), showing the first oscillation dip appeared at ~ 500 km/GeV, and interestingly enough, the error bars with red-circle showing large deficits compared with the results in the three-active neutrino framework are also well consistent with the new oscillation curve, which may be due to the existence of new sterile neutrino.

Since the high energy muon neutrinos ($10 \sim 100$ GeV) passing through the interior of the Earth are little affected by matter in this model, it is expected that the IceCube sub-detector DeepCore results [55] are similar to that provided by Super-Kamiokande atmospheric neutrino data [57] representing no evidence for light sterile neutrinos. In addition to the IceCube

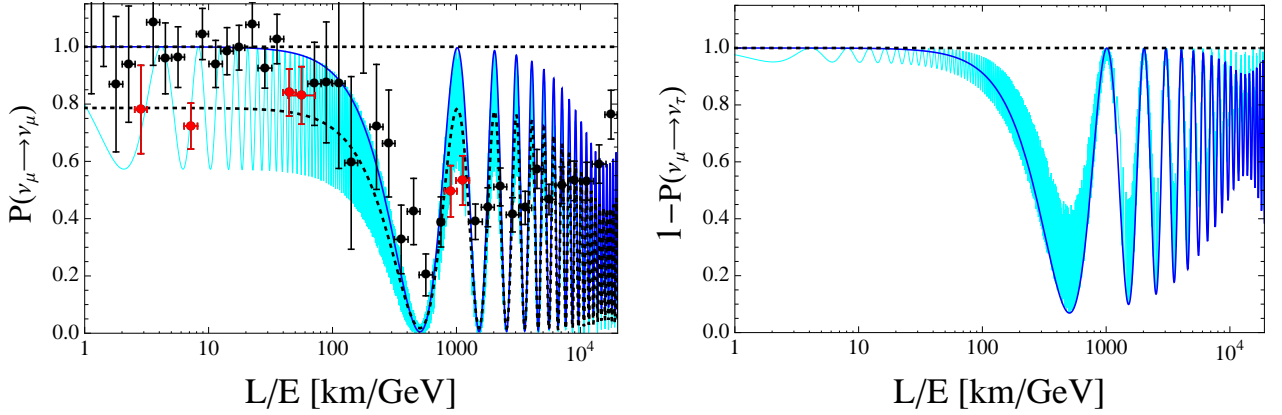


FIG. 5: Plots of $P_{\bar{\nu}_\mu \rightarrow \bar{\nu}_\mu}$ (left) and $1 - P_{\nu_\mu \rightarrow \nu_\tau}$ (right) *vs.* L/E [km/GeV], where the blue sinusoidal curves stand for the standard forms of the three-active neutrino probabilities and the black-dotted curve for $\sin^2\left(\frac{\Delta S^2_i}{4E}L\right)$ being averaged out. In the left plot the data points represent the atmospheric muon neutrino events observed in Super-Kamiokande [57].

DeepCore results [55], the track-like muon events selected in the MINOS and MINOS+ data [45] shows the first oscillation dip at ~ 500 km/GeV mainly due to the muon neutrino oscillation into not sterile neutrinos but tau neutrinos.

However, there exists a possibility to probe the existence of sterile neutrinos by comparing the results of $P_{\nu_\mu \rightarrow \nu_\mu}$ with those of $1 - P_{\nu_\mu \rightarrow \nu_\tau}$. In fact, both results are almost equivalent for the standard oscillation for the three-active neutrinos. But, they are different for the new oscillation affected by the sterile neutrinos. In the right panel of Fig. 5, we plot $1 - P_{\nu_\mu \rightarrow \nu_\tau}$, where the blue sinusoidal curve and the cyan oscillation curve correspond to the standard three-active neutrino oscillations and new oscillation with $\theta_3 = 1.28$, $\Delta S^2_{31} = 0.6 \text{ eV}^2$, respectively. In the $\nu_\mu \leftrightarrow \nu_\tau$ oscillation, the oscillation parameters are fixed to the best-fit values¹⁴ for NO given in Eq. (20). Such discrepancy between $P_{\nu_\mu \rightarrow \nu_\mu}$ and $1 - P_{\nu_\mu \rightarrow \nu_\tau}$ would be proved through both the $\nu_\mu \rightarrow \nu_\tau$ appearance experiments and the ν_μ disappearance experiments in the future. Recently, the OPERA collaboration has confirmed that muon neutrinos primarily oscillate into tau neutrinos [71]. In the case of $\tilde{m}_{\nu_3}^2 \rightarrow m_{\nu_3}^2$, as shown in Fig. 4, an MSW resonance is expected to occur in multi-GeV, similar to the standard oscillation for the three-active neutrino [22], for the atmospheric and accelerator $\nu_{e,\mu}$ neutrinos traveling in earth matter with the propagation eigenstates of active neutrinos [27].

¹⁴ As the uncertainty of θ_{23} is large its impact on the result is not negligible.

VI. IMPLICATIONS OF ICECUBE DATA.

The astrophysical neutrinos with very high energy fly galactic and extra galactic distances far beyond the earth-sun distance can give us an opportunity to probe pseudo-Dirac neutrinos with very tiny mass splittings as mentioned before. Taking into account astronomical-scale baseline satisfying $4\pi E/\Delta m_{\text{Sol,Atm}}^2 \ll L \sim 4\pi E/\Delta m_k^2$ with $k = 1, 2$ to uncover the oscillation effects of very tiny mass splitting Δm_k^2 , the probability of neutrino flavor conversion from Eq. (31) reads

$$P_{\nu_\alpha \rightarrow \nu_\beta} = \delta_{\alpha\beta} - \sum_{k=1}^2 |U_{\alpha k}|^2 |U_{\beta k}|^2 \sin^2 \left(\frac{\Delta m_k^2 L}{4E} \right) - \frac{1}{2} |U_{\alpha 3}|^2 |U_{\beta 3}|^2 \cos^2 2\theta_3 - 2 \sum_{k>j} \text{Re}[U_{\beta k}^* U_{\beta j} U_{\alpha j}^* U_{\alpha k}], \quad (50)$$

where the oscillatory terms involving the atmospheric and solar mass-squared differences and the large mass-squared differences Δm_3^2 , ΔS_{3k}^2 and ΔQ_{3k}^2 with $k = 1, 2$ are averaged out over such long distances.. As shown in [72], the matter effects inside the Gamma Ray Burst (GRB) sources as well as the earth are not significant, which makes us to consider vacuum oscillation only for astrophysical neutrinos. Neutrino telescope such as IceCube [73] observes neutrinos from extragalactic sources located far away from the earth and with neutrino energy $10^5 \text{ GeV} \lesssim E \lesssim 10^7 \text{ GeV}$. Given neutrino trajectory L and energy E , the oscillation effects become prominent when $\Delta m_k^2 \sim E/4\pi L$, where $L \equiv L(z)$ is a distance-measure with redshift z , which is different from comoving or luminosity distance, given by

$$L(z) \equiv D_H \int_0^z \frac{dz'}{(1+z')^2 \sqrt{\Omega_m(1+z')^3 + \Omega_\Lambda}}, \quad (51)$$

where the Hubble length $D_H = c/H_0 \simeq 4.42 \text{ Gpc}$ with the results of the Planck Collaboration [30]:

$$\Omega_\Lambda = 0.6911 \pm 0.0062, \quad \Omega_m = 0.3089 \pm 0.0062, \quad H_0 = 67.74 \pm 0.46 \text{ km s}^{-1} \text{ Mpc}^{-1}, \quad (52)$$

in which Ω_Λ , Ω_m , and H_0 stand for the dark energy density of the Universe, the matter density of the Universe, and the present Hubble expansion rate, respectively. The asymptotic value of $L(z)$ is about 2.1 Gpc achieved by large value of z , which means that the smallest Δm_k^2 that can be probed with astrophysical neutrinos with E is $10^{-17} \text{ eV}^2 (E/\text{PeV})$ [74]. If

this is the case, in order to observe the oscillation effects the oscillation lengths should not be much larger than the flight length before arriving at neutrino telescopes in earth for given tiny mass splittings, that is,

$$L_{\text{osc}}^k \simeq \left(\frac{5 \times 10^{-15} \text{ eV}^2}{\Delta m_k^2} \right) \left(\frac{E}{5 \times 10^5 \text{ GeV}} \right) 8 \text{ Mpc} \lesssim 8 \text{ Mpc} \quad (53)$$

which means that astrophysical neutrinos with $L \simeq 8 \text{ Mpc}$ (flight length) and energy $E \simeq 0.5 \text{ PeV}$ would be useful to probe the pseudo-Dirac property of neutrinos with the very tiny mass splitting $\Delta m_k^2 \simeq 5 \times 10^{-15} \text{ eV}^2$. From Eq. (53), we see that given the tiny mass splittings $\Delta m_k^2 = 10^{-14 \sim -16} \text{ eV}^2$ with the energies around 100 TeV–1 PeV, a new oscillation curve at neutrino trajectory $\lesssim \mathcal{O}(10) \text{ Mpc}$ is naively expected to occur.

On the other hand, oscillation effects induced by tiny mass splittings Δm_k^2 for the pseudo-Dirac neutrinos can affect the track-to-shower ratio for the number of shower N_S and track events N_T measured from IceCube experiment, which is given by [15, 16],

$$\frac{N_T}{N_S} = \frac{p_T \{a_\mu \tilde{F}_\mu - \sum_{k=1}^2 a_k^\mu \tilde{F}_k^\mu\}}{a_e \tilde{F}_e + a_\mu (1 - p_T) \tilde{F}_\mu + a_\tau \tilde{F}_\tau - \sum_{k=1}^2 \{a_k^e \tilde{F}_k^e + a_k^\mu (1 - p_T) \tilde{F}_k^\mu + a_k^\tau \tilde{F}_k^\tau\}}, \quad (54)$$

where

$$\begin{aligned} \tilde{F}_\alpha &= \sum_\beta \left\{ \delta_{\alpha\beta} - \frac{1}{2} |U_{\alpha 3}|^2 |U_{\beta 3}|^2 \cos^2 2\theta_3 - 2 \sum_{k>j} \text{Re}[U_{\beta k}^* U_{\beta j} U_{\alpha j}^* U_{\alpha k}] \right\} \phi_\beta^0, \\ a_\alpha &= 4\pi \int dE E^{-\omega} A_\alpha(E), \\ \tilde{F}_k^\alpha &= \sum_\beta |U_{\alpha k}|^2 |U_{\beta k}|^2 \phi_\beta^0, \\ a_k^\alpha &= 4\pi \int dE \sin^2 \left(\frac{\Delta m_k^2 L}{4E} \right) E^{-\omega} A_\alpha(E), \end{aligned} \quad (55)$$

with a spectral index ω , the detector effective areas $A_\alpha(E)$ and initial flavor composition ϕ_β^0 . Here p_T is the probability that an observed event produced by a muon neutrino is a track event, which is mildly dependent on energy and approximately equals to 0.8 [75]. The prediction for the ratio N_T/N_S depends on the initial flavor composition $\phi_e^0 : \phi_\mu^0 : \phi_\tau^0$ at the source which are relevant for the interpretation of observational data. There are four well-known production mechanisms for high energy neutrinos from which the flavor compositions are given: (i) $(\frac{1}{3} : \frac{2}{3} : 0)$ for π decay, (ii) $(\frac{1}{2} : \frac{1}{2} : 0)$ for charmed mesons decay, (iii) $(1 : 0 : 0)$ for β decay of neutrons, and (iv) $(0 : 1 : 0)$ for π decay with damped muons.

We confront the predictions of N_T/N_S with experimental results by taking $\Delta m_1^2 = 10^{-15} \text{ eV}^2$, $\Delta m_2^2 = 10^{-16} \text{ eV}^2$ and $\theta_3 = 1.28$ as a benchmark point as well as the best-fit values in Eq. (20) for the neutrino mixing angles and CP phase. As can be seen from

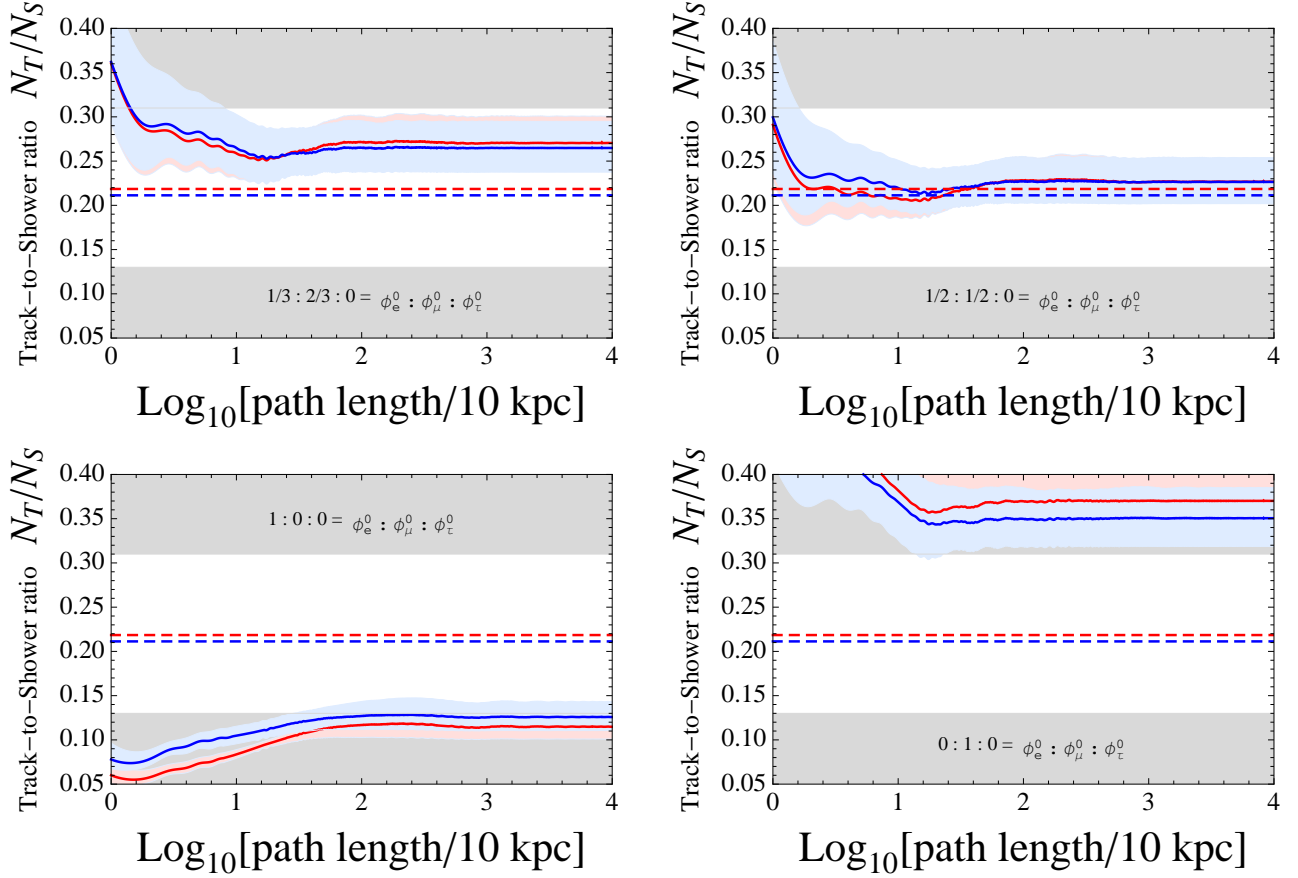


FIG. 6: Plots of the track-to-shower ratio N_T/N_S as a function of L ($\log_{10}[\text{path length}/10 \text{ kpc}]$) for NO (red curve) and IO (blue curve) with $\Delta m_1^2 = 10^{-15} \text{ eV}^2$, $\Delta m_2^2 = 10^{-16} \text{ eV}^2$ and $\theta_3 = 1.28$. Each panel corresponds to the specific initial flavor composition $(\phi_e^0 : \phi_\mu^0 : \phi_\tau^0)$ at the source. For three neutrino mixing angles and Dirac-type CP phase we take the global fit results in Eq. (20). Red and blue curved lines correspond to normal and inverted neutrino mass orderings, respectively, for $\omega = 2.2$, whereas light red and light blue regions represent the corresponding results for $\omega = 1.8 - 2.6$. Gray shaded regions are forbidden by $N_T/N_S = 0.18^{+0.13}_{-0.05}$ [15].

eqs.(54,55), the tiny mass splittings $\Delta m_{k(=1,2)}^2$ can be searched for, looking at high energy cosmic neutrinos by measuring the track-to-shower ratio N_T/N_S as the function of L ($\log_{10}[\text{path length}/10 \text{ kpc}]$).

In the numerical analysis, we use the spectral index given by $\omega = 2.2 \pm 0.4$ [75] and the best-fit values for NO (IO) in Eq. (20). Fig. 6 shows the plots of the track-to-shower ratio N_T/N_S as a function of L ($\log_{10}[\text{path length}/10 \text{ kpc}]$) for the neutrino energy $60 \text{ TeV} \lesssim E_\nu \lesssim 3 \text{ PeV}$ studied in Ref. [15]. According to four specific assumptions at each panel for

the flavor compositions at the source ($\phi_e^0 : \phi_\mu^0 : \phi_\tau^0$), for $\omega = 2.2$, $\Delta m_1^2 = 10^{-15} \text{ eV}^2$ and $\Delta m_2^2 = 10^{-16} \text{ eV}^2$ the normal (inverted) mass ordering is presented as the red (blue) curved line, whereas light red and light blue regions represent the corresponding results for $\omega = 1.8 - 2.6$. Gray shaded regions are forbidden by the measurement $N_T/N_S = 0.18_{-0.05}^{+0.13}$ [15]. In Fig. 6, we see that the oscillation effect occurs at distance $\lesssim 1.5 \text{ Mpc}$ and it is averaged out at distance beyond 1.5 Mpc . The predictions of N_T/N_S for the given inputs and the specific initial flavor compositions $1/3 : 2/3 : 0$ and $1/2 : 1/2 : 0$ are consistent with the measurement, whereas those for the other two initial flavor compositions are disfavored. In the plots, we draw the horizontal dashed lines corresponding to the cases without oscillation effects (i.e. the cases for $\Delta m_{1,2}^2 = 0$). The gap between the predictions with and without oscillations is due to the oscillatory term in eq.(50). Therefore, substantial reduction of uncertainty in the measurement of N_T/N_S would test not only the model itself but also the oscillation effects induced by pseudo-Dirac nature of neutrinos.

VII. CONCLUSION

We have proposed a convincing model containing sterile neutrinos to interpret both SBL neutrino anomalies and high energy neutrino data observed at IceCube in terms of neutrino oscillations. Different from the so-called $3 + 1$ model where the PMNS matrix is simply extended to 4×4 unitary matrix as in Refs. [19–21], the new 4×4 neutrino mixing matrix in our model is parameterized in a way to keep the 3×3 PMNS mixing matrix for three active neutrinos unitary. A characteristic feature of this model is that there are no flavor changing neutral current interactions leading to the conversion of active neutrinos to sterile ones or vice versa. We have presented new forms of neutrino oscillation probabilities modified by introducing new sterile neutrinos. In this scenario, there are new mass squared differences ($\Delta m_{1,2,3}^2$, ΔS_{31}^2) and new mixing angle θ_3 in addition to the standard oscillation parameters associated with only three active flavor neutrinos. While $\Delta m_{1,2}^2$ are responsible for astronomical baseline high energy neutrino oscillations, Δm_3^2 (or ΔS_{31}^2) and θ_3 are usable to interpret SBL neutrino oscillations.

Our model can explain SBL neutrino anomalies in terms of neutrino oscillations at the same level of $3 + 1$ model. However, there still exist small tensions (1) in the reactor and Gallium data, flux normalization and 5 MeV bump observed from $\nu_e \rightarrow \nu_e$ disappearance, (2)

between the MiniBooNE data in the region $L/E \gtrsim 1.5$ [m/MeV] and the model predictions at $\Delta S_{31}^2 = 0.6 \text{ eV}^2$ for $\nu_\mu \rightarrow \nu_e$ appearance for $\sum m_\nu$ favored by Planck Collaboration (TT+lowP) at 95% CL [31], and (3) between the Super-Kamiokandes atmospheric neutrino data and the IceCube DeepCore results including the MINOS and MINOS+ data released in Neutrino 2018 .

We have shown that resolution of the reactor antineutrino flux anomaly is required to reduce statistical uncertainties and/or to understand its underlying physics at baselines $L \lesssim 500$ m. In the present model the values of the parameters θ_3 and ΔS_{31}^2 favored by the Planck data of $\sum m_\nu \lesssim 0.705$ eV are not conflict with the NEOS and DANSS results [51] which are in a tension with the Gallium and reactor anomalies as in 3+1 model [21].

We have shown that the LSND $\bar{\nu}_e$ appearance data favors probability driven by $\theta_3 \sim 1.28$ with $\Delta S_{31}^2 = 0.6 \text{ eV}^2$ satisfying a cosmological bound $\sum m_\nu \lesssim 0.705$ eV. The MiniBooNE excess results are well consistent with the LSND data at $L/E \lesssim 1.5$ [m/MeV] while the excess of two data at $L/E \gtrsim 1.5$ [m/MeV] seems to be disfavored by a cosmological bound $\sum m_\nu \lesssim 0.705$ eV. Since the LSND and MiniBooNE data can be interpreted as $\bar{\nu}_\mu \rightarrow \bar{\nu}_e$ oscillation, experimental search for $\bar{\nu}_\mu$ (or ν_μ) disappearance would test our model in which it could be observed at $L/E \sim 1.2$ [m/MeV] with $E_{\nu_\mu} \sim 0.5$ GeV and $L = 600$ m for $\Delta S_{31}^2 = 0.6 \text{ eV}^2$ with $\theta_3 = 1.28$ in the SBN Program experiment [58]. In addition, we have studied the earth matter effect, and found that it is negligible for muon neutrinos having energies $\gg 1$ GeV when they pass through the interior of the Earth.

Finally, we have found that the existence of light sterile neutrino we consider does not affect solar neutrino oscillation and thus no constraint on new parameters came out from it. It has been shown that the Super-Kamiokande's atmospheric neutrino data are consistent with the new $\nu_\mu \leftrightarrow \nu_\tau$ oscillation affected by sterile neutrino, showing the first oscillation dip appeared at $\sim 500 \text{ km/GeV}$ which is a characteristic feature of this model. The most recent data of DeepCore [55] and MINOS and MINOS+ [45] experiments do not show any signature of light sterile neutrinos. In addition, we have shown that the probabilities of $P_{\bar{\nu}_\mu \rightarrow \bar{\nu}_\mu}$ and $1 - P_{\nu_\mu \rightarrow \nu_\tau}$ versus L/E [km/GeV] have a clear discrepancy with different oscillation signatures of light sterile neutrinos, unlike the expected from the three neutrino standard form. Such discrepancy could be probed through both the ν_τ appearance and the ν_μ disappearance experiments in the future. We have discussed the implications of the very high energy neutrino events detected at IceCube on the probe of the oscillation effects induced by two

pseudo-Dirac mass splittings.

Acknowledgments

We would like to give thanks to E. J. Chun, Xiaojun Bi, S. H. Seo, and Yufeng Li for useful conversations. Y.H. Ahn is supported by the NSFC under Grant No. U1738209.

-
- [1] M. H. Ahn *et al.* [K2K Collaboration], Phys. Rev. Lett. **93**, 051801 (2004) [hep-ex/0402017].
 - [2] P. Adamson *et al.* [MINOS Collaboration], Phys. Rev. D **73**, 072002 (2006) doi:10.1103/PhysRevD.73.072002 [hep-ex/0512036].
 - [3] Y. Fukuda *et al.* [Super-Kamiokande Collaboration], Phys. Rev. Lett. **81**, 1562 (1998) [hep-ex/9807003].
 - [4] T. Araki *et al.* [KamLAND Collaboration], Phys. Rev. Lett. **94**, 081801 (2005) [hep-ex/0406035].
 - [5] Q. R. Ahmad *et al.* [SNO Collaboration], Phys. Rev. Lett. **89**, 011301 (2002) [nucl-ex/0204008].
 - [6] F. P. An *et al.* [Daya Bay Collaboration], Phys. Rev. Lett. **108**, 171803 (2012) [arXiv:1203.1669 [hep-ex]].
 - [7] J. K. Ahn *et al.* [RENO Collaboration], Phys. Rev. Lett. **108**, 191802 (2012) [arXiv:1204.0626 [hep-ex]].
 - [8] Y. Abe *et al.* [Double Chooz Collaboration], Phys. Rev. Lett. **108**, 131801 (2012) [arXiv:1112.6353 [hep-ex]].
 - [9] G. Mention, M. Fechner, T. Lasserre, T. A. Mueller, D. Lhuillier, M. Cribier and A. Letourneau, Phys. Rev. D **83**, 073006 (2011) [arXiv:1101.2755 [hep-ex]]; P. Huber, Phys. Rev. C **84**, 024617 (2011) Erratum: [Phys. Rev. C **85**, 029901 (2012)] [arXiv:1106.0687 [hep-ph]]; J. Kopp, M. Maltoni and T. Schwetz, Phys. Rev. Lett. **107**, 091801 (2011) [arXiv:1103.4570 [hep-ph]].
 - [10] D. N. Abdurashitov *et al.*, Phys. Rev. Lett. **77**, 4708 (1996); J. N. Abdurashitov *et al.* [SAGE Collaboration], Phys. Rev. C **59**, 2246 (1999) [hep-ph/9803418]; J. N. Abdurashitov *et al.*, Phys. Rev. C **73**, 045805 (2006) [nucl-ex/0512041]; J. N. Abdurashitov *et al.* [SAGE Collab-

- oration], Phys. Rev. C **80**, 015807 (2009) [arXiv:0901.2200 [nucl-ex]].
- [11] P. Anselmann *et al.* [GALLEX Collaboration], Phys. Lett. B **342**, 440 (1995); W. Hampel *et al.* [GALLEX Collaboration], Phys. Lett. B **420**, 114 (1998); F. Kaether, W. Hampel, G. Heusser, J. Kiko and T. Kirsten, Phys. Lett. B **685**, 47 (2010) [arXiv:1001.2731 [hep-ex]].
 - [12] C. Athanassopoulos *et al.* [LSND Collaboration], Phys. Rev. Lett. **75**, 2650 (1995) [nucl-ex/9504002]; A. Aguilar-Arevalo *et al.* [LSND Collaboration], Phys. Rev. D **64**, 112007 (2001) [hep-ex/0104049].
 - [13] A. A. Aguilar-Arevalo *et al.* [MiniBooNE Collaboration], arXiv:1805.12028 [hep-ex].
 - [14] M. G. Aartsen *et al.* [IceCube Collaboration], Science **342**, 1242856 (2013) [arXiv:1311.5238 [astro-ph.HE]]; M. G. Aartsen *et al.* [IceCube Collaboration], Phys. Rev. Lett. **113**, 101101 (2014) [arXiv:1405.5303 [astro-ph.HE]]; M. G. Aartsen *et al.* [IceCube Collaboration], Phys. Rev. Lett. **114**, no. 17, 171102 (2015) [arXiv:1502.03376 [astro-ph.HE]].
 - [15] A. Palladino, G. Pagliaroli, F. L. Villante and F. Vissani, Phys. Rev. Lett. **114**, no. 17, 171101 (2015), [arXiv:1502.02923 [astro-ph.HE]]; G. Pagliaroli, A. Palladino, F. L. Villante and F. Vissani, Phys. Rev. D **92**, no. 11, 113008 (2015) [arXiv:1506.02624 [hep-ph]].
 - [16] Y. H. Ahn, S. K. Kang and C. S. Kim, JHEP **1610**, 092 (2016) [arXiv:1602.05276 [hep-ph]].
 - [17] A. Esmaili and Y. Farzan, JCAP **1212** (2012) 014 [arXiv:1208.6012 [hep-ph]]; V. Brdar, J. Kopp and X. P. Wang, JCAP **1701**, no. 01, 026 (2017) [arXiv:1611.04598 [hep-ph]]; B. Chauhan and S. Mohanty, Phys. Rev. D **98**, no. 8, 083021 (2018) [arXiv:1808.04774 [hep-ph]].
 - [18] Y. H. Ahn, Phys. Rev. D **96**, no. 1, 015022 (2017) [arXiv:1611.08359 [hep-ph]].
 - [19] R. N. Mohapatra, S. Nasri and H. B. Yu, Phys. Rev. D **72**, 033007 (2005) [hep-ph/0505021].
 - [20] S. Gariazzo, C. Giunti, M. Laveder, Y. F. Li and E. M. Zavanin, J. Phys. G **43**, 033001 (2016) [arXiv:1507.08204 [hep-ph]].
 - [21] K. N. Abazajian *et al.*, arXiv:1204.5379 [hep-ph].
 - [22] C. Patrignani *et al.* (Particle Data Group), Chinese Phys. C **40** 100001 (2016) and 2017 update.
 - [23] M. Kobayashi and C. S. Lim, Phys. Rev. D **64**, 013003 (2001) [hep-ph/0012266].
 - [24] Y. H. Ahn, Phys. Rev. D **98**, no. 3, 035047 (2018) [arXiv:1804.06988 [hep-ph]]; Y. H. Ahn, Phys. Rev. D **91**, 056005 (2015) [arXiv:1410.1634 [hep-ph]].
 - [25] C. D. Froggatt and H. B. Nielsen, Nucl. Phys. B **147**, 277 (1979).

- [26] P. Minkowski, Phys. Lett. **67B**, 421 (1977).
- [27] L. Wolfenstein, Phys. Rev. D **17**, 2369 (1978); S. P. Mikheyev and A. Y. Smirnov, Sov. J. Nucl. Phys. **42**, 913 (1985) [Yad. Fiz. **42**, 1441 (1985)].
- [28] P. F. de Salas, D. V. Forero, C. A. Ternes, M. Tortola and J. W. F. Valle, Phys. Lett. B **782**, 633 (2018) [arXiv:1708.01186 [hep-ph]].
- [29] A. de Gouvea, W. C. Huang and J. Jenkins, Phys. Rev. D **80**, 073007 (2009) [arXiv:0906.1611 [hep-ph]].
- [30] P. A. R. Ade *et al.* [Planck Collaboration], Astron. Astrophys. **594**, A13 (2016) [arXiv:1502.01589 [astro-ph.CO]].
- [31] M. Moscibrodzka, H. Falcke and S. Noble, Astron. Astrophys. **596**, A13 (2016) [arXiv:1610.08652 [astro-ph.HE]]; N. Aghanim *et al.* [Planck Collaboration], Astron. Astrophys. **596**, A107 (2016) [arXiv:1605.02985 [astro-ph.CO]].
- [32] F. Kohlinger *et al.*, Mon. Not. Roy. Astron. Soc. **471**, no. 4, 4412 (2017) [arXiv:1706.02892 [astro-ph.CO]].
- [33] C. Kraus, A. Singer, K. Valerius and C. Weinheimer, Eur. Phys. J. C **73**, no. 2, 2323 (2013) [arXiv:1210.4194 [hep-ex]]; J. A. Formaggio and J. Barrett, Phys. Lett. B **706**, 68 (2011) [arXiv:1105.1326 [nucl-ex]]; A. Sejersen Riis, S. Hannestad and C. Weinheimer, Phys. Rev. C **84**, 045503 (2011) [arXiv:1105.6005 [nucl-ex]].
- [34] C. Giunti, M. Laveder, Y. F. Li, Q. Y. Liu and H. W. Long, Phys. Rev. D **86**, 113014 (2012) [arXiv:1210.5715 [hep-ph]]; S. Goswami and W. Rodejohann, JHEP **0710**, 073 (2007) [arXiv:0706.1462 [hep-ph]]; Y. F. Li and S. s. Liu, Phys. Lett. B **706**, 406 (2012) [arXiv:1110.5795 [hep-ph]]; I. Girardi, A. Meroni and S. T. Petcov, JHEP **1311**, 146 (2013) [arXiv:1308.5802 [hep-ph]]; S. Pascoli, M. Mitra and S. Wong, Phys. Rev. D **90**, no. 9, 093005 (2014) [arXiv:1310.6218 [hep-ph]]; A. Abada, V. De Romeri and A. M. Teixeira, JHEP **1409**, 074 (2014) [arXiv:1406.6978 [hep-ph]].
- [35] M. Archidiacono, N. Fornengo, C. Giunti and A. Melchiorri, Phys. Rev. D **86**, 065028 (2012); M. Archidiacono, N. Fornengo, C. Giunti, S. Hannestad and A. Melchiorri, Phys. Rev. D **87**, no. 12, 125034 (2013); S. Gariazzo, C. Giunti and M. Laveder, JHEP **1311**, 211 (2013); J. Bergstrm, M. C. Gonzalez-Garcia, V. Niro and J. Salvado, JHEP **1410**, 104 (2014).
- [36] S. Hannestad, I. Tamborra and T. Tram, JCAP **1207**, 025 (2012) [arXiv:1204.5861 [astro-ph.CO]].

- [37] K. Abazajian, N. F. Bell, G. M. Fuller and Y. Y. Y. Wong, Phys. Rev. D **72**, 063004 (2005) [astro-ph/0410175].
- [38] R. H. Cyburt, B. D. Fields, K. A. Olive and T. H. Yeh, Rev. Mod. Phys. **88**, 015004 (2016) [arXiv:1505.01076 [astro-ph.CO]].
- [39] C. Kraus *et al.*, Eur. Phys. J. C **40**, 447 (2005) [hep-ex/0412056].
- [40] V. N. Aseev *et al.* [Troitsk Collaboration], Phys. Rev. D **84**, 112003 (2011) [arXiv:1108.5034 [hep-ex]].
- [41] S. Mertens [KATRIN Collaboration], Phys. Procedia **61**, 267 (2015).
- [42] C. Aalseth *et al.*, hep-ph/0412300.
- [43] H. V. Klapdor-Kleingrothaus, I. V. Krivosheina, A. Dietz and O. Chkvorets, Phys. Lett. B **586**, 198 (2004) [hep-ph/0404088].
- [44] M. Agostini *et al.* [GERDA Collaboration], Phys. Rev. Lett. **111**, no. 12, 122503 (2013) [arXiv:1307.4720 [nucl-ex]].
- [45] See talks at Neutrino 2018 “<https://www.mpi-hd.mpg.de/nu2018/>”.
- [46] Y. Abe *et al.* [Double Chooz Collaboration], JHEP **1410**, 086 (2014) Erratum: [JHEP **1502**, 074 (2015)] [arXiv:1406.7763 [hep-ex]].
- [47] D. Adey *et al.* [Daya Bay Collaboration], arXiv:1808.10836 [hep-ex]; F. P. An *et al.* [Daya Bay Collaboration], Phys. Rev. Lett. **116**, no. 6, 061801 (2016) Erratum: [Phys. Rev. Lett. **118**, no. 9, 099902 (2017)] [arXiv:1508.04233 [hep-ex]].
- [48] F. Boehm *et al.*, Phys. Rev. D **64**, 112001 (2001) [hep-ex/0107009].
- [49] M. Apollonio *et al.* [CHOOZ Collaboration], Eur. Phys. J. C **27**, 331 (2003) [hep-ex/0301017].
- [50] T. A. Mueller *et al.*, Phys. Rev. C **83**, 054615 (2011) [arXiv:1101.2663 [hep-ex]]; P. Huber, Phys. Rev. C **84**, 024617 (2011) Erratum: [Phys. Rev. C **85**, 029901 (2012)] [arXiv:1106.0687 [hep-ph]];
- [51] Y. J. Ko *et al.* [NEOS Collaboration], Phys. Rev. Lett. **118**, no. 12, 121802 (2017) [arXiv:1610.05134 [hep-ex]]; I. Alekseev *et al.* [DANSS Collaboration], arXiv:1804.04046 [hep-ex].
- [52] B. Armbruster *et al.* [KARMEN Collaboration], Phys. Rev. D **65**, 112001 (2002) [hep-ex/0203021].
- [53] <http://www.numi.fnal.gov>.
- [54] A. B. Sousa [MINOS and MINOS+ Collaborations], AIP Conf. Proc. **1666**, 110004 (2015)

- [arXiv:1502.07715 [hep-ex]].
- [55] M. G. Aartsen *et al.* [IceCube Collaboration], Phys. Rev. D **91**, no. 7, 072004 (2015) [arXiv:1410.7227 [hep-ex]].
 - [56] L. H. Whitehead [MINOS Collaboration], Nucl. Phys. B **908**, 130 (2016) [arXiv:1601.05233 [hep-ex]].
 - [57] Y. Ashie *et al.* [Super-Kamiokande Collaboration], Phys. Rev. Lett. **93**, 101801 (2004) [hep-ex/0404034].
 - [58] M. Bass, PoS ICHEP **2016**, 481 (2016) [arXiv:1702.00990 [physics.ins-det]].
 - [59] V. D. Barger, K. Whisnant, S. Pakvasa and R. J. N. Phillips, Phys. Rev. D **22**, 2718 (1980); E. D. Carlson, Phys. Rev. D **34**, 1454 (1986); A. Dar, A. Mann, Y. Melina and D. Zajfman, Phys. Rev. D **35**, 3607 (1987); G. Auriemma, M. Felcini, P. Lipari and J. L. Stone, Phys. Rev. D **37**, 665 (1988).
 - [60] A. M. Dziewonski and D. L. Anderson, Phys. Earth Planet. Interiors **25**, 297 (1981).
 - [61] M. G. Aartsen *et al.* [IceCube Collaboration], Phys. Rev. Lett. **117**, no. 7, 071801 (2016) [arXiv:1605.01990 [hep-ex]].
 - [62] M. Dentler, O. Hernandez-Cabezudo, J. Kopp, P. A. N. Machado, M. Maltoni, I. Martinez-Soler and T. Schwetz, JHEP **1808**, 010 (2018) [arXiv:1803.10661 [hep-ph]]; S. Gariazzo, C. Giunti, M. Laveder and Y. F. Li, JHEP **1706**, 135 (2017) [arXiv:1703.00860 [hep-ph]]; K. N. Abazajian *et al.*, arXiv:1204.5379 [hep-ph]; J. M. Conrad, C. M. Ignarra, G. Karagiorgi, M. H. Shaevitz and J. Spitz, Adv. High Energy Phys. **2013**, 163897 (2013) [arXiv:1207.4765 [hep-ex]].
 - [63] J. Asaadi, E. Church, R. Guenette, B. J. P. Jones and A. M. Szelc, Phys. Rev. D **97**, no. 7, 075021 (2018) [arXiv:1712.08019 [hep-ph]].
 - [64] V. A. Kostelecky and M. Mewes, Phys. Rev. D **69**, 016005 (2004) [hep-ph/0309025]; T. Katori, V. A. Kostelecky and R. Tayloe, Phys. Rev. D **74**, 105009 (2006) [hep-ph/0606154]; J. S. Diaz and V. A. Kostelecky, Phys. Lett. B **700**, 25 (2011) [arXiv:1012.5985 [hep-ph]]; J. S. Diaz and A. Kostelecky, Phys. Rev. D **85**, 016013 (2012) [arXiv:1108.1799 [hep-ph]].
 - [65] S. N. Gninenko, Phys. Rev. Lett. **103**, 241802 (2009) [arXiv:0902.3802 [hep-ph]]; S. N. Gninenko and D. S. Gorbunov, Phys. Rev. D **81**, 075013 (2010) [arXiv:0907.4666 [hep-ph]]; Y. Bai, R. Lu, S. Lu, J. Salvado and B. A. Stefanek, Phys. Rev. D **93**, no. 7, 073004 (2016) [arXiv:1512.05357 [hep-ph]]; Z. Moss, M. H. Moulai, C. A. Argelles and J. M. Conrad, Phys.

- Rev. D **97**, no. 5, 055017 (2018) [arXiv:1711.05921 [hep-ph]].
- [66] J. Liao and D. Marfatia, Phys. Rev. Lett. **117**, no. 7, 071802 (2016) [arXiv:1602.08766 [hep-ph]].
 - [67] M. Carena, Y. Y. Li, C. S. Machado, P. A. N. Machado and C. E. M. Wagner, Phys. Rev. D **96**, no. 9, 095014 (2017) [arXiv:1708.09548 [hep-ph]].
 - [68] K. Abe *et al.* [T2K Collaboration], Phys. Rev. D **91**, 051102 (2015) [arXiv:1410.8811 [hep-ex]].
 - [69] <http://kamland.stanford.edu>.
 - [70] S. Abe *et al.* [KamLAND Collaboration], Phys. Rev. Lett. **100**, 221803 (2008) [arXiv:0801.4589 [hep-ex]]; A. Gando *et al.* [KamLAND Collaboration], Phys. Rev. D **83**, 052002 (2011) [arXiv:1009.4771 [hep-ex]].
 - [71] N. Agafonova *et al.* [OPERA Collaboration], Phys. Rev. Lett. **120**, no. 21, 211801 (2018) Erratum: [Phys. Rev. Lett. **121**, no. 13, 139901 (2018)] [arXiv:1804.04912 [hep-ex]].
 - [72] C. Lunardini and A. Y. Smirnov, Nucl. Phys. B **583**, 260 (2000) [hep-ph/0002152].
 - [73] <https://icecube.wisc.edu>.
 - [74] A. Esmaili and Y. Farzan, JCAP **1212**, 014 (2012) [arXiv:1208.6012 [hep-ph]]; A. Esmaili, Phys. Rev. D **81**, 013006 (2010), [arXiv:0909.5410 [hep-ph]].
 - [75] M. G. Aartsen *et al.* [IceCube Collaboration], Science **342**, 1242856 (2013) [arXiv:1311.5238 [astro-ph.HE]]; M. G. Aartsen *et al.* [IceCube Collaboration], Phys. Rev. Lett. **113**, 101101 (2014), [arXiv:1405.5303 [astro-ph.HE]]; M. G. Aartsen *et al.* [IceCube Collaboration], Phys. Rev. Lett. **114**, no. 17, 171102 (2015), [arXiv:1502.03376 [astro-ph.HE]].